NASA / DLR Aeronautical Design Challenge 2021

HeRA - Hydrogen Powered Regional Aircraft

Team
M. Rodekamp, D. Helmert, J. Bölk , L. Bach, M. Lötzsch, T. Hanl

Academic Support
Dipl.-Ing. Florian Dexl
Chair of Aircraft Engineering
Technische Universität Dresden

Submission Date
July 17th, 2021

Team Members

Team members from left to right:

Jonathan Bölk
Aerospace Engineering, 6th semester (Diploma)
jonathan.boelk@mailbox.tu-dresden.de

Daniel Helmert
Aerospace Engineering, 6th semester (Diploma)
daniel.helmert@mailbox.tu-dresden.de

Marc Rodekamp (Team Leader)
Aerospace Engineering, 8th semester (Diploma)
marc_julian.rodekamp@tu-dresden.de

Markus Lötzsch
Aerospace Engineering, 6th semester (Diploma)
markus.loetzsch@mailbox.tu-dresden.de

Thomas Hanl
Aerospace Engineering, 6th semester (Diploma)
thomas.hanl@mailbox.tu-dresden.de

Luckas Bach
Aerospace Engineering, 8th semester (Diploma)
luckas_maximilian.bach@mailbox.tu-dresden.de

TECHNISCHE UNIVERSITÄT DRESDEN

Declaration of Authorship

We hereby declare that the thesis submitted is our own unaided work.
All direct or indirect sources used are acknowledged as references.

We are aware that the thesis in digital form can be examined for the use of unauthorized aid and in order to determine whether the thesis as a whole or parts incorporated in it may be deemed as plagiarism.

This paper was not previously presented to another board and has not been published.

Dresden, July 13th, 2021

Marc Rodekamp

Markus Lötzsch

Luckas Bach

Daniel Helmert

Thomas Hanl

Jonathan Bölk

TECHNISCHE UNIVERSITÄT DRESDEN

Fakultät Maschinenwesen Institut für Luft- und Raumfahrttechnik

Technische Universität Dresden, 01062 Dresden

Deutsches Zentrum für Luft- und Raumfahrt e. V. (DLR)
Institut für Aerodynamik und Strömungstechnik | Transportflugzeuge

Prof. Dr.
Johannes Markmiller
Professur für Luftfahrzeugtechnik

Bearbeiter: Florian Dexl

Telefon: 0351 463-38096
Telefax: 0351 463-37263
E-Mail: florian.dexl@tu-dresden.de
AZ: 21-12

Dresden, 14/07/2021

NASA/DLR Design Challenge: Approval and support of report submission

To whom it may concern,

As the academic supervisors, we hereby declare to approve the report written by the student team consisting of

- Luckas Bach,
- Jonathan Bölk,
- Thomas Hanl,
- Daniel Helmert,
- Markus Lötzsch,
- Marc Rodekamp

and support the submission to the NASA/DLR Design Challenge 2021. We further declare that the report is the result of the above-listed students' own work.

Best regards

TECHNISCHE UNIVERSITÄT DRESDEN
Institut für Luft- und Raumfahrttechnik
Professur für Luftfahrzeugtechnik
Prof. Dr. Johannes Markmiller
01062 Dresden

Prof. Dr. Johannes Markmiller

Dipl.-Ing. Florian Dexl

Abstract

Climate change is the biggest challenge society is facing today. The civil aviation sector contributes a significant portion to the global greenhouse gas emissions. Due to this, it is vital that the aviation industry seeks to create innovative designs with the eventual goal of reducing emissions to zero. Hydrogen possesses the potential to become the solution to the issues the civil aviation industry faces today. As an energy carrier that can be regeneratively produced from water and green energy, it could replace kerosene as the primary fuel of the aviation industry with long-term sustainability in mind.
To capture the potential of hydrogen, the student team of the *Technische Universität Dresden* has created a design for a 150 passenger regional aircraft powered by hydrogen, with a range of 2000 *km*, called *Hydrogen Powered Regional Aircraft—HeRA*. This report establishes the feasibility of *HeRA* for an entry into service by 2035 while adhering to the guidelines set by the NASA/DLR Design Challenge 2021.
HeRA uses a set of evolutionary and innovative design proposals which enable more efficient flight and the utilization of hydrogen in civil aviation. In order to increase efficiency and range an innovative wing design, the box wing, was chosen. Additionally, *HeRA* makes use of more electric flight by providing the energy for its internal components through a combination of fuel cell and battery. *HeRA* accomplishes this task while adhering to the principle of evolutionary design and maintaining interoperability with current airport infrastructure.

Zusammenfassung

Der Klimawandel ist die größte Herausforderung, der sich die Gesellschaft heute stellen muss. Der zivile Luftfahrtsektor trägt einen erheblichen Teil zu den globalen Treibhausgasemissionen bei. Aus diesem Grund ist es wichtig, dass die Luftfahrtindustrie innovative Konzepte entwickelt, um die Emissionen auf null zu reduzieren. Wasserstoff hat das Potenzial, die Lösung für die Probleme der zivilen Luftfahrtindustrie zu werden. Als Energieträger, der regenerativ aus Wasser und grüner Energie hergestellt werden kann, könnte er Kerosin als primären Treibstoff der Luftfahrtindustrie mit Blick auf die langfristige Nachhaltigkeit ersetzen.
Um das Potenzial von Wasserstoff zu nutzen, hat das Studententeam der *Technischen Universität Dresden* einen Entwurf für ein wasserstoffbetriebenes Regionalflugzeug für 150 Passagiere mit einer Reichweite von 2000 *km* erstellt, das *Hydrogen PowEred Regional Aircraft-HeRA*. In diesem Bericht wird die Machbarkeit von *HeRA* für eine Indienststellung bis 2035 unter Einhaltung der Richtlinien der NASA/DLR Design Challenge 2021 nachgewiesen.
HeRA verwendet eine Reihe von evolutionären und innovativen Designvorschlägen, die einen effizienteren Flug und die Nutzung von Wasserstoff in der zivilen Luftfahrt ermöglichen. Um Effizienz und Reichweite zu erhöhen, wurde ein innovatives Flügeldesign, der Box Wing, gewählt. Zusätzlich nutzt *HeRA* den Gedanken des mehr elektrischen Fliegens. Hierbei wird die elektrische Energie für die internen Komponenten durch eine Kombination aus Brennstoffzellen und Batterien bereitstellt. *HeRA* erfüllt diese Aufgabe unter Einhaltung des Prinzips des evolutionären Designs und unter Beibehaltung der Interoperabilität mit der aktuellen Flughafeninfrastruktur.

Contents

Nomenclature

Abbreviations

AC	Air Conditioning Unit
APU	Auxiliary Power Unit
AS	Air Start Unit
BULK	Bulk Train
CAS	Calibrated Air Speed
CAT	Catering Truck
CB	Conveyor Belt
CC	Combustion Chamber
CG	Center of Gravity
CLEAN	Cleaning Truck
CO_2	Carbon Dioxide
CS-25	Certification Specifications for Large Aeroplanes
DoH	Degree of Hybridization
EAS	Equivalent Airspeed
EASA	European Union Aviation Safety Agency
EIS	Entry Into Service
FUEL	Fuel Hydrant Dispenser or Hydrogen Tanker
GH_2	Gaseous Hydrogen
GPU	Ground Power Unit
H_2	Hydrogen
HPC	High Pressure Compressor
HTP	Horizontal Tail Plane
IR	Infrared
ICA	Initial Cruise Altitude
ISA	International Standard Atmosphere
L/D	Lift-to-Drag
LDCL	Lower Deck Cargo Loader
LH_2	Liquid Hydrogen
LPC	Low Pressure Compressor
LV	Lavatory Vehicle
MTOM	Maximum Take-Off Mass
MAC	Mean Aerodynamic Chord
MLVI	Multi-Layer Vacuum Insulation
OEW	Operating Empty Weight
PBB	Passenger Boarding Bridge
PS	Passenger Stairs
TAS	True Air Speed
TOW	Tow Tractor
TRL	Technology Readiness Level
ULD	Unit Load Devices Train
UV	Ultraviolet
VTP	Vertical Tail Plane

WV	Potable Water Vehicle

Symbol	Description	Unit
A	Area	$[m^2]$
b	Wingspan	$[m]$
$\overline{c}$	Length of MAC	$[m]$
$\overline{c'}$	Relative length of MAC	[-]
C_L	Lift coefficient	[-]
C_D	Drag coefficient	[-]
$C_{D,0}$	Zero-lift drag coefficient	[-]
C_{Dtr}	Trim drag coefficient	[-]
C_{Dp}	Profile drag coefficient	[-]
C_{Dpa}	Parasitic drag coefficient	[-]
C_{Dint}	Interference drag coefficient	[-]
C_M	Pitch moment coefficient	[-]
$C_{N,max}$	Maximum normal force	[-]
E_{opt}	Optimal glide ratio	[-]
F	Thrust	[N]
g	Gravitational acceleration	$[\frac{m}{s^2}]$
h	Horizontal distance of front wing to CG	$[m]$
h_{HX}	Enthalpy	$[\frac{J}{kg}]$
$\frac{h}{b}$	Height to span ratio	[-]
l	Horizontal distance of aft wing to CG	$[m]$
l'	Horizontal distance of the wings	$[m]$
m	Mass	$[kg]$
$\dot{m}$	Mass flow rate	$[\frac{kg}{s}]$
n	Load factor	[-]
Ma	Mach number	[-]
s	Relative reference area of the wing	[-]
S_F	Wing surface	$[\mathrm{m}^2]$
T	Temperature	$[K]$
V	Velocity	$[\frac{m}{s}]$
V_S	Stalling speed	$[\frac{m}{s}]$
V_{S+}	Stalling speed with wing-flaps retracted	$[\frac{m}{s}]$
V_G	Negative design manoeuvring speed	$[\frac{m}{s}]$
V_A	Positive design manoeuvring speed	$[\frac{m}{s}]$
V_C	Design cruising speed	$[\frac{m}{s}]$
V_D	Design dive speed	$[\frac{m}{s}]$
V_F	Design speed with extended flaps	$[\frac{m}{s}]$
V_{AF}	Design speed with retracted flaps	$[\frac{m}{s}]$

Greek

α	Angle of attack	$[^\circ]$
α_{HX}	Heat transfer coefficient	$[\frac{W}{m^2K}]$

Λ	Aspect ratio	[-]
λ	Taper ratio	[-]
ϕ	Sweep	[°]
ϑ	Temperature	[°C]
ϑ_F	Temperature fluid	[°C]
ϑ_W	Temperature wall	[°C]

List of Figures

List of Tables

1 Introduction

The European Union introduced the Green Deal in 2020 in order to facilitate the decarbonization of the European economy. An important area of this drive is the aviation industry which contributes 2-3% of all human-made carbon emissions. Of the carbon emissions of the aviation industry, 50% is attributed to the low range sector with distances of less than 3000 km. Therefore a large focus must be put on developing new concepts for this sector to reduce overall carbon emissions.
Taking this into account, a hydrogen-fueled short-range airplane has great potential in allowing the industry to reach climate neutrality [1].

2 Design Overview

Hydrogen Powered Regional Aircraft - HeRA was developed to meet the future requirements of clean aviation. With elegant and proven solutions, *HeRA* will enable the civil aviation industries to take off into the future. Besides a hydrogen refueling system, *HeRA* requires no additional infrastructure and integrates perfectly with existing systems.
HeRA possesses an elegant box wing design allowing it to operate at maximum efficiency and giving future passengers the opportunity to see revolutionary concepts at work. At the same time, a traditional dual-engine setup provides familiarity to both passengers and air carriers. Electrical power will be provided through a combination of fuel cells and batteries which replaces conventional methods that require high maintenance on conventional aircraft. Resistant foam tanks are installed for the safe storage of hydrogen, while an intelligent system of heat exchangers and heating elements replaces the use of complex pumps. In addition, *HeRA* spares no expense in making hydrogen-fueled aviation as safe as possible. All systems have been designed to be redundant providing maximum safety for passengers. The innovative landing gear system further provides extended safety by protecting from tailstrikes while still allowing for conventional boarding and deplaning. *HeRA* is furthermore able to carry 150 passengers in a pure economy configuration.

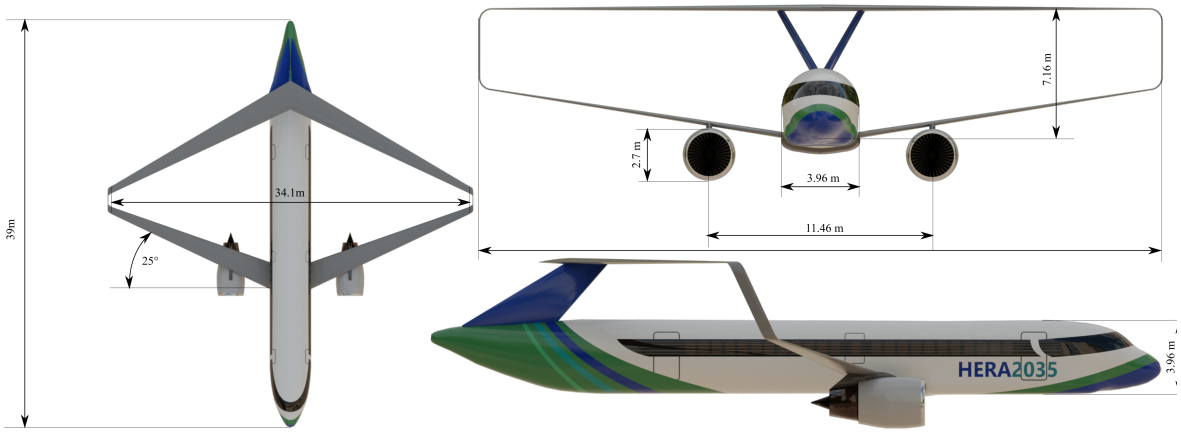

Figure 1: Orthographic projection

Table 1: Plane geometry

Parameter	Value
Fuselage	
Height	10 m
Length	38.98 m
Wing	
Wingspan	34.1 m
Area	120 m^2
Aspect ratio	9.69
Dihedral (top)	0°
Dihedral (bottom)	9°
Sweep (top)	-25°
Sweep (bottom)	25°
Tail unit area	22.6 m^2

2.1 Initial Calculation and Sizing

In order to enable initial calculations and to conduct a preliminary study into key design parameters of *HeRA*, a reference plane had to be found. For this purpose the Airbus A320neo was chosen due to its key mission parameters. Its passenger capacity of 150-180 and range of 6000 km are sufficiently similar to the design requirements of 150 passengers and a range of 2000 km. It is also a member of the latest generation of civilian passenger aircraft and as such is sufficient as a comparison to potential future aircraft in 2035, especially as its performance with 30% sustainable aviation fuel was evaluated.
Based on the data from the A320neo listed in Table 16 and the design requirements laid out, an initial study of the fuel mass required was conducted. The study investigated the feasibility of the different powertrain configurations of electric, hybrid-electric, and combustion, at an optimal lift-to-drag ratio and their impact on the total mass of potential airplane concepts. The degree of hybridization of the aircraft is defined as the amount of electric power to the total amount of power used for thrust.

$$\text{DoH} = \frac{\text{Electric Power}}{\text{Total Power}} \cdot 100\%. \tag{1}$$

At a DoH of 0%, all thrust would be generated by H_2 combustion while at a DoH of 100% all thrust would be generated through electric power, produced by a fuel cell. Each powertrains characteristics were investigated at a range of 2000 km, based on the Brequet Range equation [2]. Based on these results a fully electric system utilizing hydrogen fuel cells was discarded due to the mass required for its powertrain being too large to allow for a competitive design. Following this, a total of 6 preliminary design concepts were created and investigated based on their projected advantages and disadvantages. Due to the introduction year of 2035, an evolutionary design was chosen utilizing a narrow-body dragon configuration while providing improvements to the aerodynamic properties over conventional designs through the use of a box wing. Following studies focused on the feasibility of an electric-hybrid powertrain of different degrees of hybridization. The preliminary design process is displayed in Figure 37.

2.2 Propulsion Method

After the initial determination of the configuration was completed, the feasibility of pure hydrogen combustion and a hybrid solution, consisting of both hydrogen combustion and electric propulsion through fuels cells were investigated. The results from figure 2 show that with an increase of hybridization, the total weight is increased while enabling a reduction of fuel consumption. Therefore an optimal design targets the highest possible degree of hybridization. However, the thermodynamic feasibility has to be taken into account as well, when trying to maximize the degree of hybridization. Therefore a thermodynamic model is introduced.

2.2.1 Hybrid Electric

The target of the investigation was to find the highest DoH. With an efficiency of $\eta = 60\%$ fuel cells generate large amounts of waste heat [3]. This waste heat can either be dissipated into the environment or be used to preheat the LH_2. The amount of heat that can be dissipated into the environment is mainly governed by the equation for forced convection.

$$\dot{Q} = \alpha_{HX} \cdot (\vartheta_F - \vartheta_W) \cdot A \tag{2}$$

While the amount of heat that can be used for preheating is limited by

$$\dot{Q} = c_p(T) \cdot \dot{m} \cdot \Delta T \tag{3}$$

[4]. The total amount of heat that can be dissipated is the sum of these heat flows. The Area A for the forced convection was defined for two cases. The ideal case where the plane could dissipate heat over the whole hull and the best case that assumes that we could dissipate heat over the whole wing area. During the investigation, it was first examined to only use LH_2 as a heat sink for the fuel cell. It became apparent, that while hydrogen has a high specific heat capacity of $c_p = 9.668 \frac{J}{gK}$ [5], the amount of heat that can be transferred to the hydrogen is not sufficient to keep the fuel cell at acceptable temperatures. As such heat dissipation over the hull or the wings of *HeRA* was added to the investigation. The results are presented in figure 3.

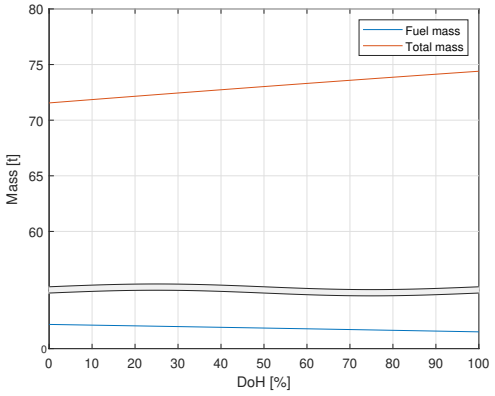

Figure 2: Masses over degree of hybridization

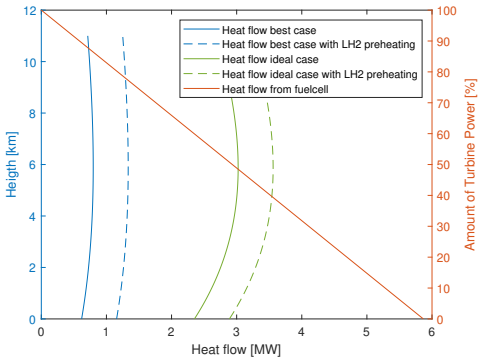

Figure 3: Heat dissipation

Figure 3 shows the results of the model. The heat dissipation is displayed for the ideal and best case. The model takes the convective dissipation of heat and the preheating of the LH_2

into account. The intersection between the heat flow line and the heat flow from the fuel cell for the best case is the design point. At the design point, DoH=10% is reached. To increase the DoH, an increase of bleed air, circulation of cooling water, and a refrigerant cycle were investigated. Further investigations showed air to be insufficient due to high mass flow rates. Water and a refrigerant cycle initially showed promising results. However, water cooling was discarded due to the excessive weight of the system while the usage of a refrigerant was rejected due to its toxicity, flammability, or ecologically harmfulness. The investigation found that for an EIS 2035 a hybrid electric model is not feasible.

2.2.2 Gas Turbine

Hydrogen Gas turbines utilize the combustion of hydrogen to generate thrust. This propulsion method is already tried and tested, with kerosene-fueled turbines being commonly used in civil aviation. Hydrogen turbines have already been successfully tested for an A320 which was refitted with an APU designed to utilize hydrogen [6]. From the TU-155 it is known that H_2 can be used in the main engine as well [7]. As a result of these aspects and the difficulties already outlined with alternative propulsion methods, a hydrogen-fueled gas turbine was chosen for *HeRA*.

2.3 Landing Gear

Using the box wing design comes with some changes regarding the landing gear. The A320neo, like most commercial aircraft, uses a tricycle landing gear. This includes one nose wheel and the main wheels under the wing. The latter have a certain vertical distance to the longitudinal axis providing lateral stability, with the center of gravity between nose wheel and main landing gear. However, *HeRA's* lower wing is positioned in front of the center of gravity. The main landing gear still has to be positioned under the wing to achieve the afore-mentioned lateral stability. Therefore, a single aft gear is introduced, while the nose wheel becomes obsolete. Since the main landing gear still has to absorb the loads during touchdown, the aft wheel is designed as a tailwheel-type landing gear, which can extend after touchdown to bring the aircraft in a horizontal position. As the tailwheel-type landing gear is positioned directly behind the aft tank, a tailstrike is impossible and the tank is always protected. After being extended, the aircraft is in the normal horizontal position and can be boarded in a conventional fashion.

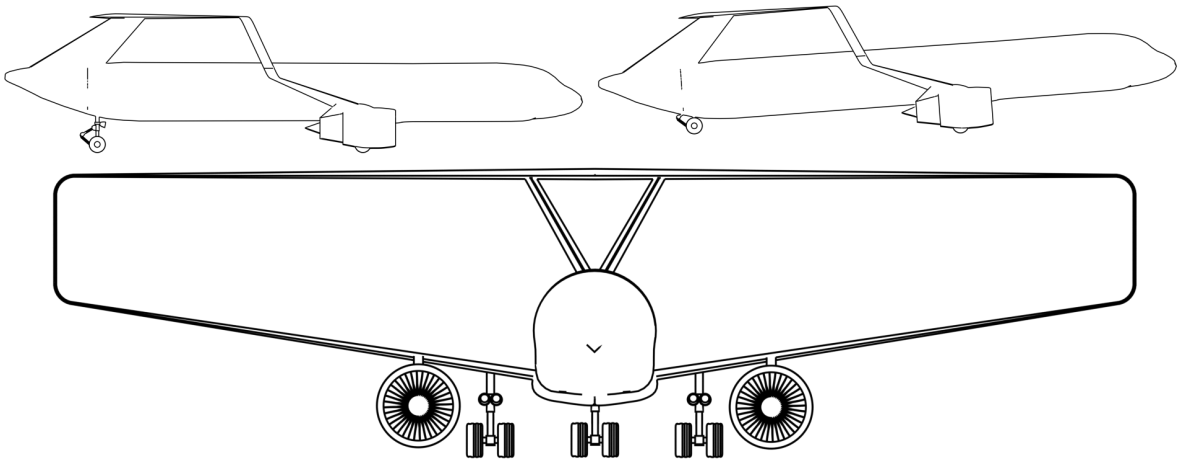

Figure 4: Side view with extended and retracted tailwheel and front perspective

Figure 4 shows *HeRA* with and without the aft wheel being extended. There is no mandatory regulation for ground clearance but the engine inlets are the most critical parts of the aircraft when it comes to ground contact. Therefore, the positioning and sizing of the engines and main landing gear were derived from the A320neo.

2.4 Cabin

HeRA can accommodate 150 PAX in a pure economy layout. A 3-3 configuration is used. An additional option is a two-class cabin layout which may transport a total of 132 PAX. A schematic of an economy layout can be found in Figures 23 and 5 and a two-class layout in Figures 22 and 25 in Appendix A.4. Both layouts use 4 toilets and 2 galleys.
Furthermore, *HeRA* is equipped with 4 Type A fore and aft exits as well as 2 Type III emergency exits mid-fuselage according to the requirements of the CS-25 [8].

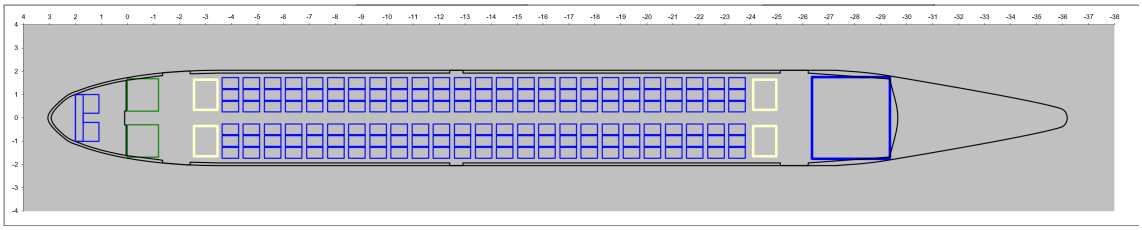

Figure 5: One-class cabin layout (150 PAX) - Green: galley; Yellow: lavatories; Blue behind cabin: aftward H_2 tank

2.5 Loadpaths - Stringers and Frames

HeRA uses a Semi-Monocoque design, meaning the skin is used to accommodate structural loads. Stringers and frames are used as load-bearing components of the framework. The stringers are responsible for transferring aerodynamic loads from the skin onto the frames. Figure 6 and 7 show a schematic visualisation of the structural design of *HeRA*. As clearly visible, the forward tanks are located in front of the wingbox. Stringers and frames are covering the inside of the fuselage. Figure 7 shows the aft LH_2 tank, located in front of the vertical stabilizer. The vertical stabilizer, which also connects to the box wing, is strapped to stringer and frames inside the tail cone, similar to today's airliners.
To allow a maximized tank volume, the forward tanks are pushed to the side, creating a bulge on each fuselage side. Thereby a third, middle tank can be installed.

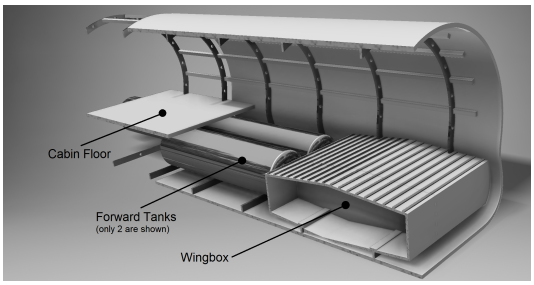

Figure 6: Schematic visualisation of front fuselage section

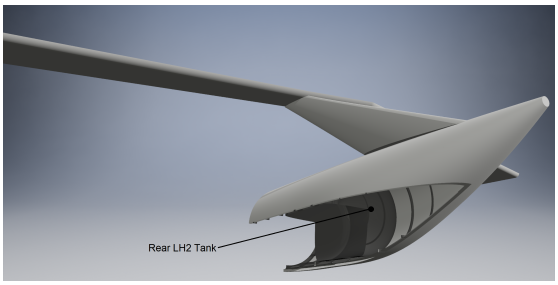

Figure 7: Schematic visualisation of tail fuselage section

2.6 Mass Breakdown

Table 2: Component mass breakdown - calculated using LTH methods [9]

	HeRA $[kg]$	A320neo $[kg]$	Δ $[kg]$
Fuselage	9200	8790	410
Wing/box wing	9000	8550	450
VTP	870	540	330
HTP	0	670	-670
Nacelles & pylon	1500	1030	470
Landing gear	3000	2850	150
Cryotank	3800	0	3800
Tank insulation	600	0	600
Tank system	2000	0	2000
Structural Weight	**29970**	**22430**	**7540**
Operational items	5300	6450	-1150
Propulsion group	7200	6920	280
Furnishings	2900	3500	-600
Aircraft systems	4700	5000	-300
Operational Empty Weight	**50070**	**44300**	**5770**
Max. payload	15750	18000	-2250
Max. fuel	2300	21360	-19060
Maximum Zero Fuel Weight	**65820**	**64300**	**1520**
Maximum Take-Off Weight	**68120**	**78000**	**-9880**
Payload for design mission (2000 km)	15750	15750	0
Fuel, including reserve, for design mission (2000 km)	2300	6200	-3900
Take-Off Weight Design Mission (2000 km, 150 PAX)	**67540**	**64270**	**3270**
Fuel, including reserve, for design mission (600 km)	830	3000	-2170
Take-Off Weight Design Mission (600 km, 150 PAX)	**66650**	**61070**	**5580**

The fact that *HeRA*'s landing weight will not differ from the take-off weight as much as with today's kerosene-fueled aircraft has to be taken into account. Due to the high energy density of hydrogen, only 1720 kg, including reserve fuel, are needed for the design mission, compared to 6200 kg of kerosene. This leads to a smaller difference between take-off and landing weight. As a result, the landing gear is designed to be stronger compared to an A320neo. Only a portion of the maximum fuel is needed for the design mission, reserve fuel included, which means with a total storage of 2300 kg, *HeRA* is able to cover distances up to 2800 km and thereby exceeds the design requirements.
For the calculation of the reserve fuel the following conditions were taken into account:

- fuel for 30 min flight at 1500 ft at half cruise speed $\rightarrow$ 212 kg
- fuel for 200 nm at maximum take-off weight at 20000 ft $\rightarrow$ 237 kg
- 5% of the required fuel mass for the design mission $\rightarrow$ 85 kg

$\rightarrow$ Total hydrogen reserve fuel mass: 534 kg

3 Aerodynamics

To achieve minimal environmental impact, *HeRA* has to fly as efficiently as possible. An efficient flight is defined by the optimal usage of the energy which is provided in our design by the used box wing configuration.
During flight, the lowest possible drag was aimed for. The drag of the plane is calculated using formula 4 [2].

$$C_{D,tot} = C_{Dp} + \frac{C_L^2}{\pi \Lambda e} + C_{Dtr} + C_{Dint} + C_{Dpa} \tag{4}$$

Aside from profile drag the two next highest sources of drag are induced drag and parasitic drag [2]. Reducing these two was a primary design goal for *HeRA*. The induced drag forming at the wing tip as a result of vortex systems is proportional to the square of the lift coefficient C_L. To reduce induced drag the aspect ratio λ and the Oswald efficiency number e are optimized. An overview of *HeRA*'s aerodynamical values can be found in Table 20 in Appendix A.6.

3.1 Box Wing

Table 3: Comparison of a conventional wing, C-wing and box wing

Wing design	Conventional	C-wing	Box wing
Structural integrity	regular	less stiff	stiffer [10]
Induced drag reduction	0%	20% [11]	30% [12]
Span efficiency e	<1	1.45 [12]	1.46 [12]

Amongst the configurations in Table 3, the box wing was found to be the best choice. The box wing reduces the induced drag for a given span, which makes up about 40% of the total drag. During take-off and landing, this share increases up to 80-90% [12]. For short-haul flights, take-off, and landing accounts for large portions of the flight. Due to this, the induced drag has a significant impact on the operational range. Therefore, the box wing allows for greater ranges and improves overall performance. For a given wingspan, the box wing can achieve a high level of efficiency. An ideal box wing, which has half the lift on both wings of a conventional reference aircraft with the same geometric properties can reduce the induced drag by up to 30% [12]. Furthermore, box wing configurations create a lower bending moment than usual cantilever-like wings [13]. In contrast to comparable aircraft, *HeRA* does not include tanks inside the wings. Therefore the dimensions are only defined by the aspects of aerodynamics and structural stability. Using the box wing configuration with its reduced loads has the potential to further reduce the weight of the wings if all wing parameters are chosen properly. A detailed list of configuration parameters can be found in Table 17 in Appendix A.2.

3.2 Aerodynamics and Drag

As seen in formula 4, the two main parameters to reduce the induced drag are the aspect ratio and the span efficiency. *HeRA's* configuration was derived from the Airbus A320neo as the reference aircraft. For the initial calculations, both the wingspan and the wing area remained the same, but the reference wing was split into two wings with identical geometry forming the box wing. This approach is carried out according to [14]. From there an optimization of the aspect ratio and span efficiency was performed. To compare the span efficiency of the box

wing and the reference configuration, a numeric approach is used, with $\frac{h}{b}$ being the height to span ratio.

$$\frac{D_{i,box}}{D_{i,ref}} = \frac{e_{ref}\Lambda_{ref}}{e_{box}\Lambda_{box}} = \frac{0.44 + 0.9594 \cdot \frac{h}{b}}{0.44 + 2.219 \cdot \frac{h}{b}} \tag{5}$$

[15] This relation also considers interference effects of both wings. If both wings were calculated separately or assuming an infinite vertical distance between them, the drag reduction would be even higher. However, especially downwash effects play a big role and are one of the disadvantages of this configuration. The height to span ratio $\frac{h}{b}$ represents the vertical gap between the fore and aft wing [15]. An optimal height to span ratio of 0.2 was chosen. The span of the reference aircraft of 34.1 m was not changed. As a result, the height between the fore and aft wing is 6.82 m which is relatively small. With a fuselage diameter of 4 m, a comparatively small V-tail is required, which also reduces drag.

Table 4: Aerodynamic values - *HeRA* and A320neo

Parameter	*HeRA*	A320neo
$C_{L,cruise}$	0.86	0.472
$C_{D,0}$	0.019	0.019
E_{opt}	21.59	18.26

To compute the zero-lift drag coefficient $C_{D,0}$, the tool OpenVSP was used. "OpenVSP is a parametric aircraft geometry tool. OpenVSP allows the user to create a 3D model of an aircraft defined by common engineering parameters."[16] After creating the model, the OpenVSP's implementation of the panel method was used to simulate the aerodynamic behavior. This method is valid for the subsonic speed and gives sufficient results for the preliminary design. Based on our configuration, a $C_{D,0}$ was calculated which is very close to the one of the reference plane. This observation is also supported in [14] since most geometrical dimensions like the fuselage size, wing area, and wingspan are similar to those of the A320neo. The typical lift-to-drag ratio of a box wing is about 20 [17]. The L/D ratio of *HeRA* and of the A320neo is shown in figure 9. It displays that *HeRA* possesses an 18 percent higher L/D ratio than the A320neo. The maximum L/D ratio is reached at an altitude of 11,950 m and has a value of 21.590. This value can be expressed by the equation

$$E_{Opt} = \frac{1}{2}\sqrt{\frac{\pi\Lambda e}{C_{D,0}}} \tag{6}$$

Based on these values, a possible airfoil thickness was calculated with the goal of achieving the highest possible profile thickness to chord length ratio $\frac{t}{c}$. This was done to maximize the structural integrity. Nevertheless, due to the box wing configuration, the absolute wing thickness is comparatively small, which brings aerodynamic benefits. However, because of the structure, the goal is to maximize thickness. A box wing has a higher stiffness so thinner wings can be used here compared to conventional wings. The airfoil thickness was calculated according to the methods of D. Schicktanz and D. Scholz [14]. The maximum feasible $\frac{t}{c}$ of *HeRA* is 0.119. It was decided to use an asymmetrical airfoil instead of a symmetrical airfoil. Additionally, it was considered whether to use a laminar wing for *HeRA*. The idea was discarded because of the laminar posture in commercial aircraft and the discontinuities on the upper side of the wing. These arise, for example, from gaps for rudders and flaps or from soling of the leading edge [2].

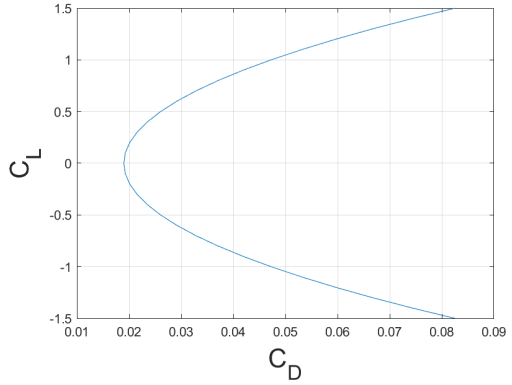

Figure 8: Lift-to-drag Polar of *HeRA*

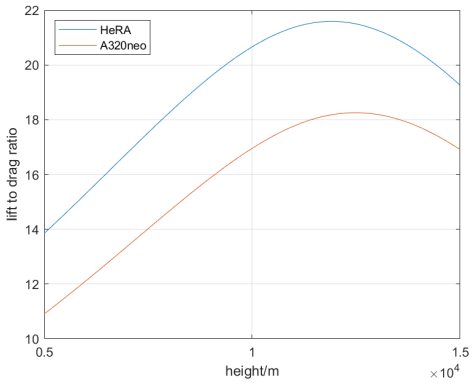

Figure 9: Lift-to-drag ratio over the height

3.2.1 Lift Behavior

To determine the influence of the angle of attack α on the lift, the empirical formula 7 suggested by [14] was used:

$$\frac{dC_L}{d\alpha} \approx \frac{2\pi A}{2 + \sqrt{A^2(1 + tan^2\varphi_{50} - Ma^2) + 4}} \tag{7}$$

To calculate the $C_L - \alpha$ and $C_D - \alpha$ characteristic, the zero-lift angle of the airfoil α_0 is needed. Although no particular airfoil was chosen for the aircraft, a comparison of different airfoils with the above-calculated t/c of 12% suggests that $\alpha_0 \approx -2.5°$, which could be provided e.g. by the NACA 2412 airfoil [18]. Therefore, the lift behavior can be expressed as follows:

$$C_L = \frac{dC_L}{d\alpha}(\alpha - \alpha_0) \tag{8}$$

3.2.2 Drag Behavior

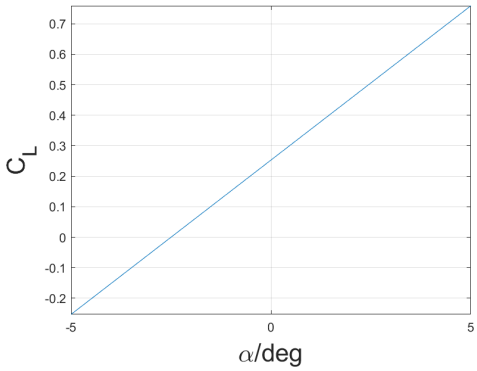

Figure 10: C_L over angle of attack

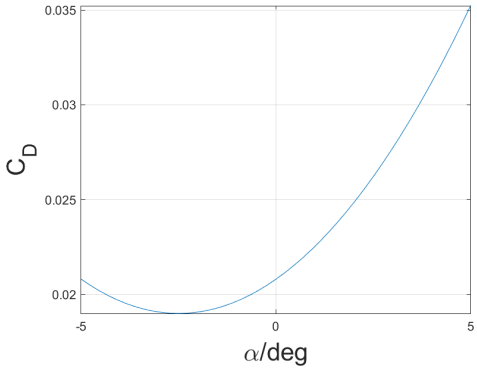

Figure 11: C_D over angle of attack

With the aspect ratio Λ and the span efficiency e determined above, the drag polar of the aircraft can easily be calculated with the known formula:

$$C_D = C_{D0} + \frac{C_L^2}{\pi e \Lambda} \tag{9}$$

It should be noted that the other drag components listed in equation 4 are neglected because of their small contribution.

3.3 Wing Geometry

3.3.1 Sweep

Aerodynamically, swept wings are only needed for transonic or supersonic speeds. Therefore, sweep is not necessary for *HeRA*. However, swept wings with an angle of 25° and -25° for the fore and aft wing respectively were chosen to allow a higher vertical distance between the upper and lower wing (see chapter 3.4). Due to this, the vertical connectors may be shortened, resulting in lower drag.

3.3.2 Taper

The taper ratio λ as the ratio of the chord lengths at tip and root of the wing has different effects on the aircraft structure and flight behavior. It determines the distribution of the local lift coefficient. A small λ, which results in a greater chord length at the wing root, reduces the bending moment of the wing and can therefore reduce the weight. However, the lower chord length may lead to stall at the wing tips even at lower speeds. This can cause instability of the aircraft. A lower chord length also means a lower Reynolds number at the wing tip, which may have negative effects on the aerodynamic behavior as well [2]. A taper ratio of $\lambda = 0.25$ was chosen, motivated by the comparison of a number of existing aircraft.

3.3.3 Dihedral

Dihedral describes the vertical angle between the wing root and wing tip. It has an effect on the roll stability of the aircraft [2]. However, it is mainly used for "fine-tuning" the flight behavior and is not exactly determined at the preliminary design phase. During the design of *HeRA* the dihedral was set to provide a proper clearance angle between the wings and the ground.

3.4 Stability

Achieving longitudinal stability for the box wing is a major challenge, which is the primary reason for conducting a stability analysis. Figure 12 shows the cross section of the MAC (c). At the MAC, the moment and the lift of the front and rear wing are displayed. The assumption was made that both wings are viewed at the same height, thus all horizontal forces are neglected. The indices 1 and 2 are assigned to the front and the rear wing respectively [15].

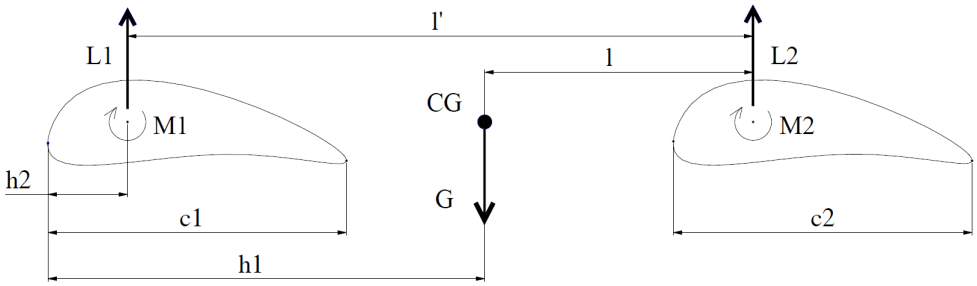

Figure 12: Sketch of box wing stability analysis [19]

As explained by D. Schicktanz and D. Scholz [14], the most important points for stability are that $C_{L,1} > C_{L,2}$, a sufficient distance between the fore and aft wing and an adjustment of wing twist and sweep. To allow a box wing to be stable and controllable, the control limit must be situated in front of the stability limit. Because of this, the control limit is defined by the forward limit and controllability requirements. The aft limit, which is also the neutral point, is defined by the stability requirements [19]. The wings generate a negative pitching moment, so for a controllable aircraft, the box wing needs a positive pitching moment around the center of gravity [19]. In the preliminary design phase, many variables are still subject to change. For example, the exact location of the center of gravity highly depends on the structural design of the aircraft and the aerodynamic coefficients are characteristic for each airfoil, which can not be determined at this point. Making detailed and specific calculations for stability and controllability would pretend an unrealistic certainty. However D. Schiktanz and D. Scholz [19] [15] prove, that a stable and controllable box wing configuration for an aircraft of our size is possible and provide a detailed discussion of the necessary considerations. The most important conclusions are that the front wing has to produce a higher lift than the aft wing, that the range for positioning of the center of gravity is relatively small and that a great horizontal distance between both wings is desired. *HeRA* possesses a V-tail. It serves to stabilize the rear flight structure, while also providing control surfaces. In order to make the center of gravity suitable for the entire wing configuration, the shape of the V-tail was swept forward [17]. The front and rear wing are used for high-lift devices and control surfaces. The slats are attached to the leading edge of the wing and the flaps and elevator are attached to the trailing edge of the wing. The aileron is on the rear wing.

3.5 Flight Manoeuvering and Gust Envelope

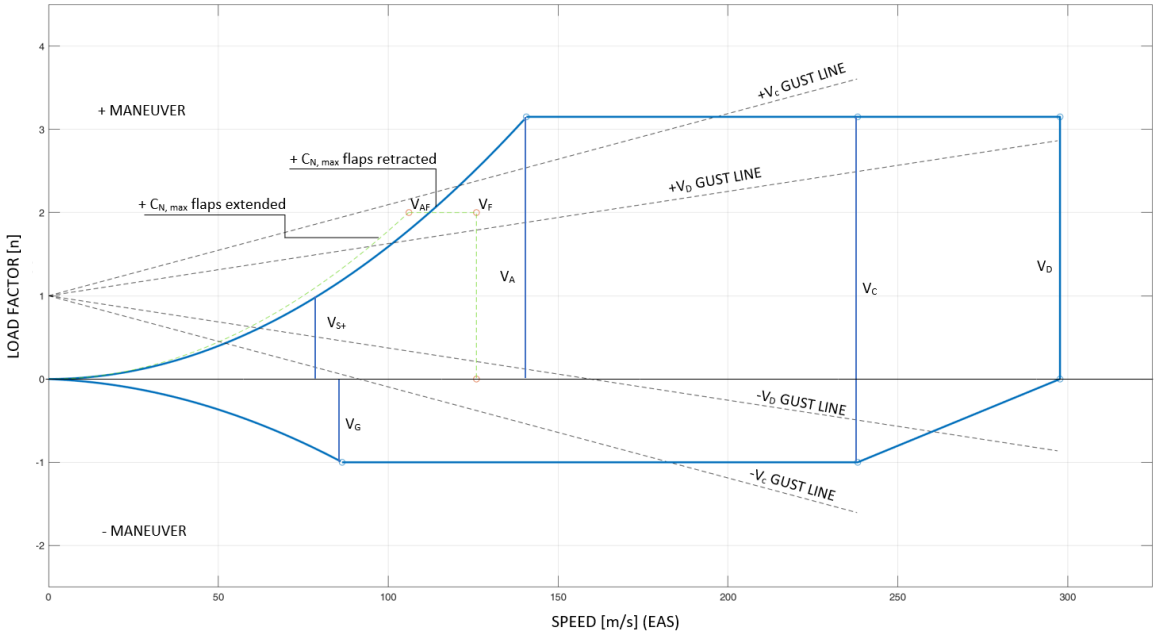

Figure 13: Flight manoeuvring and gust envelope

The calculation of the "load factor" - "flight speed" space, short V-n diagram, was designed on the basis of the EASA Airworthiness Standards. Due to the high take-off mass ($> 8618\ kg$) and the turbine-powered aircraft, the CS-25 [8] was used for *HeRA*. In addition, the gust

lines were determined. The maneuver area can be found in the Appendix figure 26. All calculations were made according to CS 25.333 and the following.

4 Powertrain

4.1 Propulsion

Even though the total efficiencies of conventional aircraft engines $\eta_{ges} \approx 40\%$ in comparison to electric technologies like the fuel cell with around $\eta_{ges} \approx 60\%$ is significantly lower, it was found that the current and upcoming generations of fuel cells produce too much heat even during cruise to be viable to drive an electric engine [3]. Preliminary investigations showed that the only feasible option is more electric flight as proposed in the report by McKinsey [20]. The detailed energy consumption of the powertrain was taken into account in the section Mission Analysis.

4.2 Layout

Based on thermodynamic calculations different layouts for the powertrain were investigated. For these investigations, the substance databases CoolProp [21] and NIST [22] have been used. To evaluate the thermodynamics a MATLAB script was developed. The script utilizes a python wrapper for CoolProp. The basic energy balance was performed for each component using the following equation:

$$\dot{Q} = \dot{m} \cdot \Delta h_{HX}(p, T) \tag{10}$$

The parameters for the enthalpy, pressure, and temperature were derived from the intake conditions of the fuel cell and the combustion chamber. For the valves, isenthalpic expansion was assumed. The extracted mass flow needed from the engine was calculated with equation 3. The layout in figure 14 has been found to be the most efficient, needing the least amount of extracted air.
Figure 14 shows the connection of all components to each other. It does not represent the position of the components in the plane. The position of components with the aircraft is shown in Figure 15. The fuel cell and engine are fed by four H_2 tanks. The H_2 is extracted by heating elements inside the tank structure. In car manufacturing, this concept has been proven and has the additional advantage that no pumps are required [23]. After reaching the system pressure of around 26 *bar* a pressure valve opens and lets the now supercritical H_2 escape. The H_2 moves in insulated pipes first through an electric heater. The 26 *bar* is two times the pressure in the combustion chamber, required for safe ignition [24]. The electric heater heats the H_2 to around 70 K. This is a safety mechanism to move the H_2 away from its critical point. Near the critical point strongly fluctuating physical properties exist, where small changes in temperature cause huge changes in the behavior of the fluid [22]. To avoid damaging components like the heat exchanger due to very high local temperature increases, an electric system is used which can react fast and reliably, and provide the right temperatures at the outlet. After the H_2 is preheated to around 70 K bleed air is extracted from the HPC. The bleed air is used to heat the H_2 up to 504 K. The mass flow is then split. The majority of H_2 is burnt in the combustion chamber, while the rest moves through an expansion valve. The H_2 and air are relaxed in such a way that they enter the fuel cell in the right working conditions [3]. The mass flow extracted in the HPC is bigger than the actual air needed for the fuel cell. The additional air extracted is used to cool the fuel cell and provide heat for the air-conditioning of the airplane. The wastewater from the fuel cell

is used for wastewater applications.

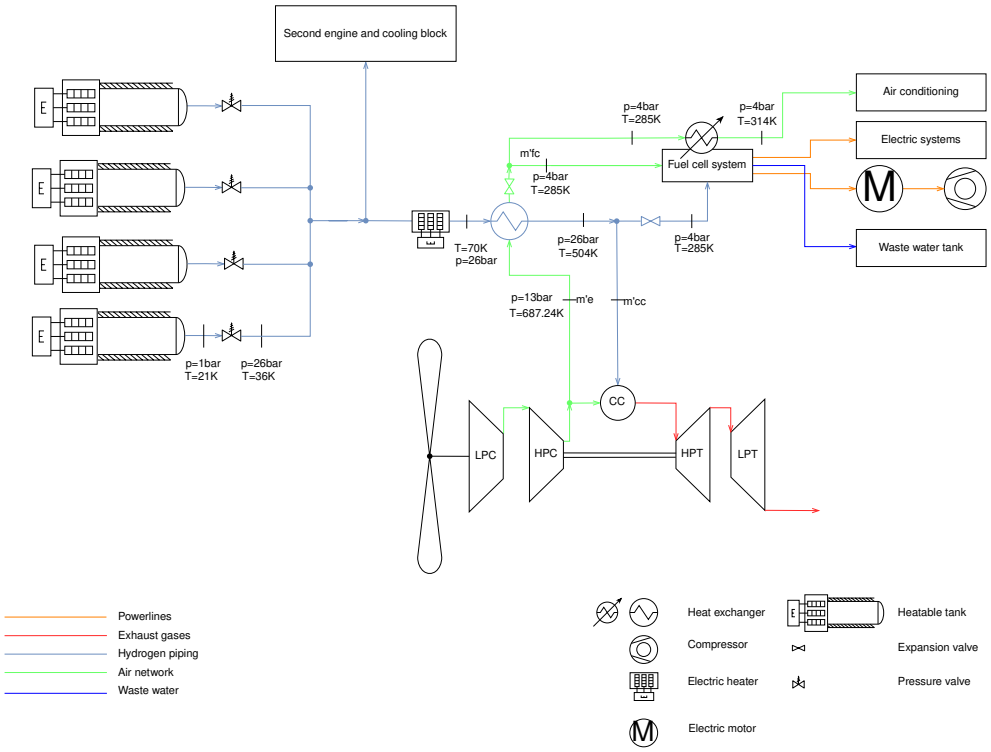

Figure 14: Powertrain

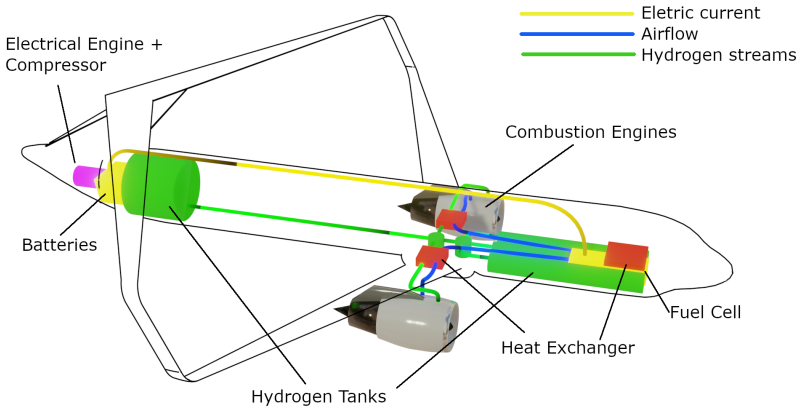

Figure 15: Position of different system components

4.3 Fuel Cell

To introduce a more ecological-friendly flight, the design was optimized to reduce the number of components that are powered by combustion processes. Two key technologies were found and replaced by a fuel cell and batteries. First the auxiliary power unit and second the electric generator in the propulsion system itself. The APU is a small gas turbine, which is used for the engine start. It powers a compressor, which blows air to the engine [2]. The APU does not provide any thrust but still consumes up to 1.4 kg/s fuel. It is predicted that

narrow-body aircraft which utilize this kind of APU will represent 70% of planes by the year 2034 [25]. *HeRA's* design counteracts these developments and allows aircraft companies to shape a cleaner future. To size the fuel cell, the power consumption for every mission step was derived using CeRAS [26]. Two cases were investigated. In the first case, the fuel cell was designed to completely compensate the APU power generation and provide sufficient energy for the electrical subsystems. During the second case, the fuel cell was designed to only supply sufficient energy for the subsystems with an additional battery system for peak loads during take-off. The results of the investigation, shown in Figure 36 in Appendix A.9, showed that a system that utilizes both a fuel cell and an advanced lithium-ion battery is favorable over a pure fuel cell design. The fuel cell with an additional lithium-ion battery is significantly lighter than using only the fuel cell. It is important to note that in the case of a pure fuel cell design, an additional battery would be needed to compensate for fast fluctuating power consumption [27]. The fuel cell system incorporates two fuel cells for redundancy.

4.4 Engines

Table 5 shows the advantages (+) and disadvantages (-) of potential engines types fueled by hydrogen for *HeRA*. The different aspects are evaluated for a flight with Ma = 0.7 at a cruise altitude of 9144 m (30000 ft). Turbofan engines were chosen for *HeRA* as their efficiency is highest for these flight missions. In addition to this passenger acceptance for this type of engine is very high and due to its extensive use in modern civil aviation technological readiness by 2035 is not in question.

Table 5: Comparison of aircraft engines [28]

Type	Noise	Specific fuel consumption	Price	Maintenance	Passenger acceptance	Technology readiness 2035
Turbojet	- - -	-	++	+	-	+
Turbofan	+	++	- -	-	+++	+++
Turboprop	- -	+	-	-	- -	++
Propfan	- - -	++	- -	-	- -	-

The chosen turbofan engines were configured based on the required thrust for take-off and landing as well as the resulting take-off and landing field length. These field lengths were calculated according to the CS-25 [8] and are displayed in Table 13.
With a total thrust of 33.77 kN during cruise flight at 9144 m altitude, the turbofan engines have an efficiency of 43% [29].

4.5 Component Efficiencies and Masses

Table 6 shows the efficiencies and Table 7 the masses of each component of the powertrain.

Table 6: Efficiencies of powertrain components

Component	Efficiency [%]
Fuel cell	60 [3]
Engine	43 [29]
Electric engine	95 [30]
Compression efficiency	80 [28]
Battery	95 [31]

Table 7: Masses of powertrain components

Component	Mass [kg]
Fuel cells	250
Engines	3000
Electric engine	100
Batteries	350
Pipes (with insulation)	200
Cryotank	3800
Tank insulation	600

5 Hydrogen

5.1 Hydrogen Characteristics

Hydrogen is a new type of energy carrier, allowing for the efficient storage and utilization of energy [1]. Table 8 compares different energy carriers for aviation. Hydrogen's advantageous high gravimetric energy density [32] and disadvantageous low density can be seen there.

Table 8: Comparison of possible fuel options [32]

Properties	LH_2	GH_2 (700 bar)	Kerosene
Gravimetric energy density	33000 Wh/kg	33000 Wh/kg	11900 Wh/kg
Density	70.8 kg/m^3 (20 K)	40 kg/m^3 (273 K)	800 kg/m^3
Volumetric energy density	2700 Wh/l	1320 Wh/l	9500 Wh/l

High-temperature combustion of hydrogen results in no CO_2 emissions and the NO_x emissions are small compared to other energy carriers [33]. During fuel cell usage only water is produced [32].

5.2 Hydrogen Storage

Initially, three different methods of hydrogen storage were assessed. Those are the storage in gaseous or liquid state, as well as the storage in a solid state, especially as metal hydrides.

5.2.1 Pressurized Hydrogen

Usually, hydrogen pressure tanks operate at 700 *bar* and room temperature. The use of a pressure tank is always a trade-off between high pressure to achieve a greater gravimetric energy density and an increasing tank weight that is needed to withstand the resulting structural loads. There is a variety of materials suitable for building a pressure tank, the most promising being carbon composites. Most of the tank materials require additional liner material to prevent the diffusion of hydrogen through the tank walls [34].

5.2.2 Solid State Storage

Another option is storage in a solid state, or more specifically, as metal hydrides. Hydrogen is capable of forming metal hydride compounds with several metals or metallic alloys. The

metal absorbs the hydrogen molecules which are then arranged inside the metal lattice. This is an exothermic reaction, thus heat is needed to release the hydrogen. Waste heat from the propulsion systems can be used for this purpose. Different metals change the optimal operating pressure and temperature as well as the density of the hydrogen stored [35]. Generally speaking, metal hydride hydrogen storage allows for much higher density compared to other means of storage. However, the ratio of hydrogen mass per tank structure mass is very low which is a big disadvantage for avionic use [34].
Other storage possibilities like carbon nanotubes and glass microspheres [34] were not considered further, since research and development is in the early stages and EIS in 2035 seems unlikely for these technologies.

5.2.3 Liquefied Hydrogen

Liquefied hydrogen (LH_2) does not require high pressure tanks, but rather has to be stored at a temperature below 21 K and at 1 bar in cryogenic tanks. These tanks and also all cryogenic pipes and valves must be highly insulated to minimize boil-off. LH_2 has a higher density compared to pressurized hydrogen which results in lower tank volumes but handling can be difficult [34].

5.2.4 Comparison and Conclusion

Table 9 compares all three storage types. The gravimetric energy density considers the weight of both the storage system and the hydrogen. Furthermore, it has to be taken into account, that because of the low density of hydrogen, the tank volume compared to kerosene is about 4 times higher for LH_2 and about 7 times higher for GH_2.
Metal hydrides, although having the highest density and therefore taking up the least space, have a far higher mass per energy unit and are therefore not suitable for aviation. The cryogenic tank storing liquid hydrogen outperforms the pressure tank both in terms of mass per energy unit and tank volume. A bigger tank requires a bigger aircraft structure, which will increase both weight and drag. Cryogenic tanks are a well-developed technology, with liquid hydrogen being used as rocket fuel for many years, where big, light, and reliable tanks are as crucial as they are for airplanes. The necessary insulation will be discussed in the next section. Also, the liquefying process requires a lot of energy [29] which needs to be taken into account when it comes to an emission comparison between LH_2-powered aircraft and commonly used powertrains.

Table 9: Comparison of hydrogen storage types

Storage type	Characteristics	H_2 density	H_2 mass per structure mass	Gravimetric energy density
Pressure tank	700 bar, 298 K [34]	39 kg/m^3 [35]	14.6% [36]	15.38 MJ/kg
Cryogenic tank	1 bar, 13 K [34]	70 kg/m^3 [36] [34]	30-68% [37]	27.78-47.62 MJ/kg
Metal hydrides	2-8 bar, 298-573 K [35]	150 kg/m^3 [35]	0.36-0.68% [34]	0.43-0.81 MJ/kg

5.3 Insulation Methods

Three types of insulation were discussed: Vacuum insulation, multi-layer vacuum insulation (MLVI), and foam insulation (polyurethane foam). Other insulation methods such as perlite insulation or mineral wool insulation were not discussed as they have much higher densities [37] or do not fit the following requirements. As requirements were set: a low price, good insulation, low mass, easy installing, safety regards, and a high technology readiness level.

Table 10: Characteristics of insulation methods [37] [38]

Insulation method	Density $[kg/m^3]$	Thermal conductivity $[mW/m*K]$	External loads tolerable?
Vacuum	50-60	0.004	No
Polyurethane foam	35	19	Yes
MLVI	50-60	0.05 - 0.02	No

In the Table above, it can be seen that vacuum- and multi-layer insulation are not suitable if they have to tolerate external loads and are nearly twice as heavy as foam insulation. But they provide a much lower thermal conductivity. To choose the right insulation it is also necessary to make sure that the insulation fits all requirements. Table 11 shows the positive and negative aspects of each insulation.

Table 11: Advantages and disadvantages of different insulation methods [37] [38]

Advantages of vacuum	Disadvantages of vacuum
-lowest thermal conductivity -high TRL	-high mass -vacuum pumps necessary -if vacuum is lost, the insulation becomes nearly useless -vulnerable to external loads

Advantages of MLVI	Disadvantages of MLVI
-low thermal conductivity -high TRL	-very expensive -extremely accurate manufacturing necessary -if vacuum is lost, the insulation becomes nearly useless -vacuum pumps necessary -high mass -vulnerable to external loads

Advantages of foam	Disadvantages of foam
-very lightweight -easy to install (spray foam) -highest TRL -very cheap -highest safety margin	-least thermal conductivity, but still good enough if the thickness is great enough

A 15 cm thick polyurethane foam insulation was chosen, because of its safety margin, easy handling and installation, the low density, the high TRL, and its low costs. A thickness

between 10-20 *cm* should be considered, with 15 *cm* being the sweet spot between weight and insulation properties [37].
As safety is one the most important and most vulnerable key aspects in the aircraft industry, a safe tank design is indispensable and with foam insulation being the only safe insulation method so far, the answer, which method to choose, was made easy. Similar reports came to the same conclusion and even Boeing's Phantom Eye (LH_2-powered unmanned aircraft) uses several foam insulated tanks [38].

5.4 Total Energy Consumption

Table 12 shows all efficiencies, from production to consumption of liquid hydrogen as fuel in *HeRA*. This calculation assumes energy is only used for thrust to fulfill the flight mission. Smaller subsystems and their efficiencies were not taken into account. Additionally the energy actually required to provide 1 joule of energy in the aircraft for the flight mission is listed.
The total efficiency of 84% for liquefaction, transportation, and storage depends heavily on multiple factors, such as ambient temperature, transportation routes, means of transport, size of the airport as well as how well the hydrogen infrastructure is developed in general. Also, the loss during the refueling process is a factor that has to be considered in future developments.
Electrolysis was chosen as a production method due to its potential of creating green hydrogen when renewable energy is used. A recent study concluded that, by 2030, the price of green hydrogen could match the one of the currently mostly used grey and blue hydrogen in an area like Australia with access to huge quantities of renewable energies [39].

Table 12: Efficiencies of LH_2 fuel

	Efficiency [%] [29]	Additional Energy [J]
Energy needed in flight		1.00
Hydrogen combustion	43	1.33
Liquefaction, transport and storage	84	0.44
Electrolysis of water	80	0.69
Total efficiency	28.90	
Total energy per joule		3.46

This sums up to a total efficiency of 28.90% and 3.46 joule needed for 1 joule of energy used in flight. Additional energy, which is not directly used for the flight mission, such as for ground support or electricity and air in the cabin, is not included.

5.5 Hydrogen Safety

To allow general acceptance of *HeRA* it must be shown that the hydrogen can be safely handled. For this purpose safety concerns primarily during and right before and after flight will be considered here. The primary aim of the safety efforts should be to prevent any leakage of hydrogen as well as to prevent ignition if hydrogen does leak [40].
To prevent hydrogen leakage, regular inspections need to be performed on the tanks and pipes filled with hydrogen. To combat leakage during a flight, monitoring systems need to be installed within the cabin to identify leakage quickly. To avoid the chance of inhalation by passengers or accidental ignition, proper ventilation needs to be installed. The leaking tank must be vented to avoid further GH_2 from entering the cabin [40].
The characteristics of hydrogen make it behave very differently than kerosene. Hydrogen

has a high ignition temperature and will not be ignited by a lighted cigarette. However, its properties also mean that it will ignite with only a tenth of the energy of other fuels. A small spark is sufficient to ignite hydrocarbon fuels in the air [40]. As such it is vital that electrical components are properly isolated and lines are inerted before and after venting of potentially leaked hydrogen. While the thermal energy radiated by hydrogen flames to the environment is lower than kerosene, the flame itself is invisible to the naked eye. Because of this factor flight and maintenance staff needs to be properly trained. UV and IR detection methods must be provided.
As LH_2 requires very low temperatures to be able to be stored high care needs to be taken to ensure that the tank materials and valves can withstand the low temperatures. Also, any traces of air or moisture within the liquid hydrogen storage may lead to freezing and clogging [40]. Due to this factor anti- or de-icing methods need to be applied to valves to ensure operability.

5.6 Tank Design

The tanks are covered with a 15 cm thick foam insulation. *HeRA* has four tanks, all within the fuselage. Three tanks are located in front of the wing, below the passenger deck, inside today's storage compartment. One, wider, tank is located behind the passenger cabin.
All front tanks have an outer diameter of 1.15 m (including wall and foam). Two tanks are 8 m long, in between them there is another 4 m tank. Also, a fuel cell is located between the two longer tanks, in front of the 4 m tank. These 3 tanks, store 10 m^3 of LH_2.
Behind the passenger cabin, a 3.5 m wide and 3 m long tank is located, which stores 23.4 m^3 of LH_2.

5.7 Hydrogen Infrastructure

5.7.1 Airport Supply

Supplying airports with hydrogen is a logistical challenge, since hydrogen production facilities are only profitable if they are operated on a large scale, and thus there are often large distances between airports and existing production facilities. As such onsite production and liquefaction of hydrogen is the best option for large airports. For smaller airports as well as at the beginning of the transitioning phase to hydrogen as a fuel, trailer trucks are the most flexible option. Ships, railway, or a pipeline system are also valid options [41].
Transporting cryogenic hydrogen is difficult, as strong insulation is required to reduce boil-off losses. Thus it makes the vehicles needed for transportation and especially pipelines for LH_2 very expensive. However, liquid hydrogen has the advantage over gaseous hydrogen that its density is much higher and therefore a lower volume needs to be transported. It is also possible to supply an airport with gaseous H_2 and liquefy it onsite. This is particularly suitable if the airport site has access to cheap and sustainable energy in large quantities. Otherwise, the LH_2 is directly liquefied at the hydrogen production facility and then transported to a main cryogenic storage tank at the airport.

5.7.2 Refueling

There are currently two primary ways of refueling aircraft at airports. Both can, in principle, also be used for refueling with liquid hydrogen, although completely new technologies are required.
It is possible to use underground refueling hydrant pipelines at the airport, which distribute

the liquid hydrogen from a main tank or liquefaction facility directly to the gates where the aircraft are refueled. However, as this option is very expensive, it is only suitable for large airports with a large number of hydrogen aircraft in service. With the prospect of introducing the first hydrogen aircraft in 2035, this will not yet be a given. In the long-term, however, direct distribution of the fuel to the gates is desirable, as it eliminates the need for additional ground transportation.
Aircraft can also be refueled with special refueling trucks that can safely transport the cryogenic fuel from a main tank or liquefaction facility to the aircraft without major losses. Due to the density and energy density of liquid hydrogen, twice as many refueling trucks are needed to refuel an aircraft than for conventional fuels. This can put a lot of strain on existing ground infrastructure, especially at large airports which have to service large amounts of planes. At small airports, this is less of an issue. Refueling trucks for LH_2 require completely different designs than conventional refueling trucks, as they must be heavily insulated. Therefore, great investment in this technology, as well as the associated safety concepts will be required for large-scale future use.
Refueling an aircraft with LH_2 is possible with a volume flow of around 900 l/min, just as with conventional jet fuel. However, due to the different densities, a larger volume must be refueled. To compensate for this and to speed up the refueling process, it is therefore imperative to refuel via several hoses at the same time. If that is not possible, turn-over time will be longer compared to conventionally powered aircraft [1]. Before the actual refueling process, it is also necessary to remove all air out of the fuel system by flooding the pipes and tanks with an inert gas [42].
Hoses used for refueling LH_2 have a much larger diameter and weight because of the thick insulation and higher pressure. This makes them more difficult to handle and accordingly may require mechanized arms to use. This may be integrated directly in a refueling truck [40]. Besides fueling, it is also important to be able to safely drain the hydrogen tanks of *HeRA*.
During fueling the primary danger comes from component failures such as valves, pipes, and sealings. As such special attention needs to be taken towards proper maintenance. The pressure and temperature of the LH_2 need to be controlled during the refueling process to prevent back-flow and minimize boil-off. Large efforts will need to be expended to ensure no ignition is possible in the case of a leakage. Although hydrogen dissipates quickly in the air. Still, ground staff needs to be retrained to safely handle the new fuel. IR or UV sensors can be used to identify hydrogen fires early on [40]. Due to these unique challenges in hydrogen refueling, ground support costs for *HeRA* will be 3 to 5 times more expensive than comparable conventional aircraft [43].

6 Mission Analysis

In order to ascertain the economic feasibility of *HeRA* while providing the least ecological impact, a mission analysis is required. Based on these requirements two mission profiles will be examined. A mission at a range of 600 km with a focus on the least ecological impact and a mission at a range of 2000 km with the least ecological impact and an economic analysis.

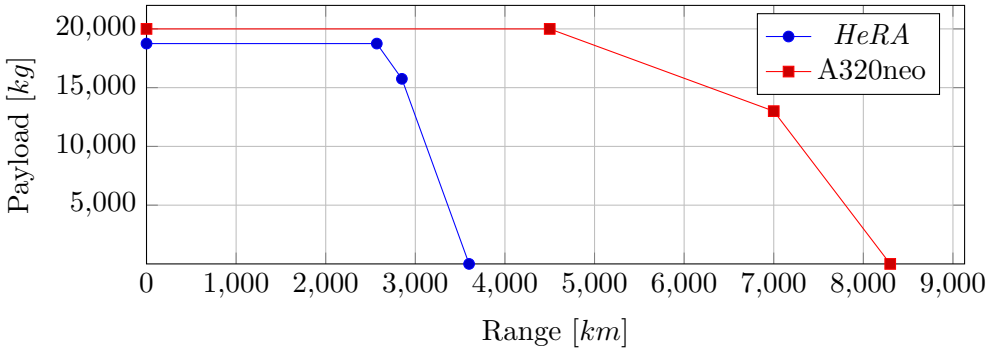

Figure 16: Payload range diagram of *HeRA* and A320neo

6.1 Calculation Approach

A 2-dimensional flight model (height and distance) was used to calculate time, energy consumption, and emissions for each segment of the flight. The behavior of an aircraft is characterized several interdependent variables, therefore it is not possible to describe the whole flight in a few analytical formulas. For example, during the ascend, the aircraft's Mach number, height, air pressure, sonic speed, temperature, thrust, and weight are all values that influence each other. The approach was to iteratively calculate these variables in a finite number of steps. The input variables, e.g. pressure, thrust, and aircraft mass are calculated at the beginning of each step and then held constant until the next iteration so that the aircraft behavior could be described with linear equations of motion in between each step. By setting the step size small enough, one can approximate the true aircraft dynamics to the needed accuracy. However, for the general mission analysis, a relatively small number of steps already gives sufficiently accurate results. This computation was implemented in MATLAB, using the ISA standard atmosphere as the model for atmospheric data. The model only considers the horizontal and vertical motion of the aircraft and does not take wind into account.
The flight is divided into a number of segments, each characterized by a start height, an end height, and a variable describing the velocity, either the true airspeed (TAS), the calibrated airspeed (CAS), or the Mach number. Take-off and landing were calculated separately, so the flight starts and ends at a height of 1,500 ft. The segments are calculated according to the script of the lecture "Conceptual Aircraft Design" at Dresden University of Technology [44]. Each section and the calculation approach are explained in detail in Appendix A.8. The values calculated with the MATLAB simulation resemble the fuel masses calculated with the Breguet range equation and actual flight durations, which validates the method. However, with the iterative approach, the necessary fuel and time for each segment as well as the $h(t)$, $v(t)$, and $h(s)$ profile can be easily calculated and plotted.

6.2 Key Mission Parameters

Table 13 shows the calculated key mission parameters for *HeRA* with the A320neo as a reference. The calculations were made for the longer 2000 km mission.
With a thrust of 130 kN per Engine, *HeRA* has a significantly shorter take-off field length than the A320neo. The landing field length is bigger than the one of the A320neo, because less fuel mass is carried and used during the flight mission, which results in a bigger landing mass.

Table 13: Key mission parameters

Mission parameter	*HeRA*	A320neo
Take-off field length $[m]$	1739	1943
Landing field length $[m]$	1535	1443
Climb rate $[\frac{m}{s}]$	31.9	32.7
Cruise speed [Mach]	0.7	0.82
Cruise altitude $[m]$	9,144	11,900
L/D (cruise)	19.7	16.9

6.3 Emissions

During hydrogen combustion, the primary emissions are water and NO_x.
NO_x is created through the reaction of atmospheric nitrogen and oxygen in high temperatures in the combustion chambers of the aircraft. For a hydrogen-fueled aircraft the emission index for NO_x is 3.08 to 14.0 $\frac{g(NO_2)}{kg(LH_2)}$ [45]. This is a decrease of over 60-90% in comparison to kerosene-fueled aircraft. However, there are techniques such as the low NO_x Micro-Mix hydrogen combustion principle which could further reduce NO_x emissions in the future [46]. In following calculations a conservative value of 14.0 $\frac{g(NO_2)}{kg(LH_2)}$ is used.
The emission of water is generally unproblematic for personal health but still poses environmental challenges. The emission index of water is 9 $\frac{kg(H_2O)}{kg(LH_2)}$ which is an increase of about 250% over kerosene planes. Due to the higher water vapor emission, the forming of contrails increases by about 1.56 on average with as much a 2 times in the tropics [45].
In comparison, kerosene emits 3.1 $\frac{to(CO_2)}{to(Kerosene)}$[47], 1.26 $\frac{kg(H_2O)}{kg(Kerosene)}$ and 12.6 $\frac{g(NO_2)}{kg(Kerosene)}$ [45].
To accommodate for the usage of 30% sustainable aircraft fuel a best-case scenario of algae-based fuel was assumed. This reduces the CO_2 emissions for the respective mass of fuel by 124% as algae absorb large amounts of CO_2 during their lifetime, allowing their total CO_2 emissions to be below zero [48].

6.4 Flight Missions

Two flight missions were analyzed. A mission with a range of 600 km and a mission with a range of 2000 km. The data for each mission can be found in Table 14 and 15.

Table 14: Parameters of 600 km mission

				Emissions	
Segment	Time $[min]$	LH_2 mass $[to]$	Energy $[MWh]$	H_2O $[to]$	NO_x $[kg]$
Ascend	4.52	0.196	6.47	1.76	2.74
Cruise	27.60	0.213	7.03	1.91	2.98
Descend	19.00	0.056	1.85	0.5	0.78
Total	51.12	0.465	15.35	4.18	6.51

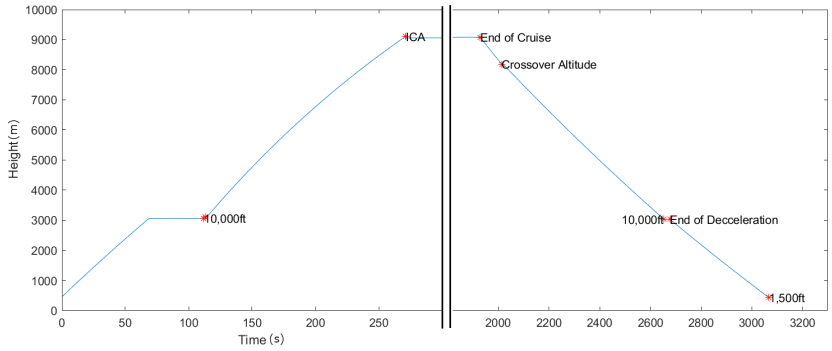

Figure 17: Flight profile of the 600 km mission

The reference plane A320neo needs 1.675 to of kerosene for the same mission which equals 19.93 MWh of energy. This equals a total emission of 3.31 to of CO_2, 2.1 to of H_2O, and 21.1 kg of NO_2. The emission of NO_2 can be drastically reduced by using different air-fuel ratios. At a ratio of 1.5 the NO_2 emissions are the highest and can be reduced by using higher or lower ratios [49].

Table 15: Parameters of 2000 km mission

				Emmissions	
Segment	Time [min]	LH_2 mass $[to]$	Energy $[MWh]$	H_2O $[to]$	NO_x $[kg]$
Ascend	4.52	0.196	6.47	1.76	2.74
Cruise	137.36	1.052	34.72	9.46	14.73
Descend	19.18	0.057	1.88	0.51	0.8
Total	161.06	1.305	43.07	11.73	18.277

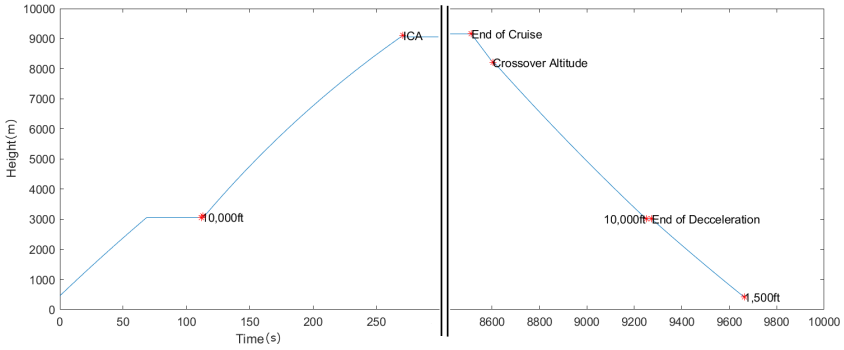

Figure 18: Flight profile of the 2000 km mission

The mission with the range of 2000 km approaches the maximum operable range of *HeRA* as the remaining fuel is reserved as reserve fuel for emergencies. The reference plane A320neo needs 4.689 to of kerosene for the same mission which equals 55.80 MWh of energy. This equals a total emission of 9.27 to of CO_2, 5.9 to of H_2O, and 59.08 kg of NO_2. For both missions the total energy consumption of *HeRA* is lower then for the reference plane.

6.5 Economic Analysis

The analysis of the direct operating cost has been conducted through the methods of J. Thorbeck from the TU Berlin [50]. The Parameters were used according to Table 18 within

Appendix A.3. Most parameters were set according to the recommendations made within the calculation method with a few notable exceptions. The Block Time Supplement per flight has been estimated to be 1 h and 13.5 min in section 6.6. This value is increased to 1.5 h as a conservative estimation of unforeseeable events and delays. The price of hydrogen is set to decrease to 2-3 USD per kg under average conditions [51]. Using the conservative estimation and utilizing a conversion ratio of 0.83 € per 1 USD the price of fuel was set at 2.5 € per kg. In addition, the price of the plane based on the OEW has been multiplied by a factor of 1.5 to 100 million € in order to be more comparable to the listed price of the reference plane of 83 million € [52]. Based on these parameters an average utilization of 1092 flights per year has been calculated resulting in an average of 3.65 departures per day which is less than the average utilization of narrow-body aircraft in 2019 of 4.33 departures per day [53]. The final Direct Operating Cost per year is 24,258,633.54 € resulting in an operating cost of 4035.57 € per blockhour. Figure 19 shows that most air carriers operating the A320neo have similar reported direct operating costs as those projected for *HeRA*. In addition, an approximation of the economic viability of the recycling of *HeRA* has been conducted using primarily statistical data of existing narrow-body airframes. Aircraft disposal costs are around 10% of the purchase price leading to an estimated disposal and recycling cost of 10,939,090 € [54]. The average salvage value of a narrow-body aircraft with two engines is 6,900,000 € [54]. As the projected value of the salvage is lower than the projected cost induced by recycling it is not economically viable to recycle *HeRA*.

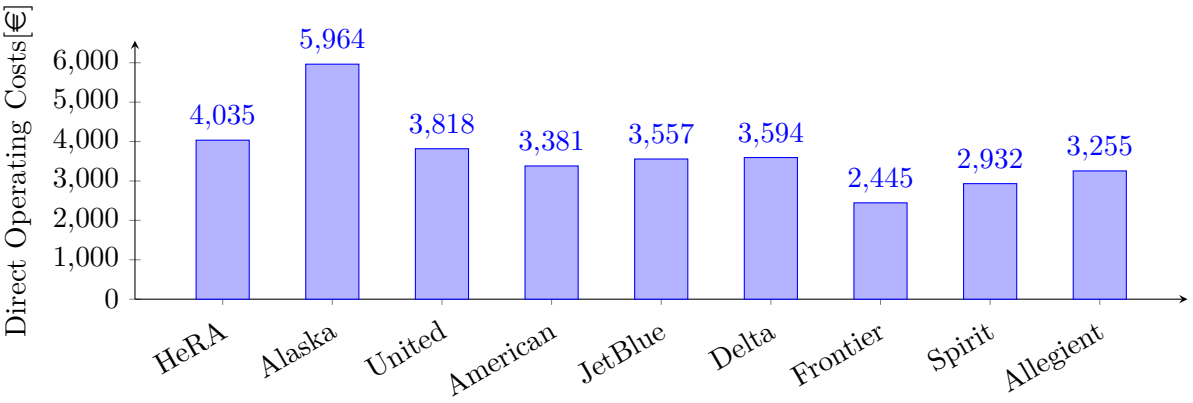

Figure 19: Comparison of various aircarriers operating the A320neo with *HeRA* [55]

6.6 Ground Operations

The ground operation of *HeRA* hardly differs from a conventional aircraft. The official Aircraft Characteristics A320neo [56] from Airbus is used for the analysis. The stand safety line delimits the aircraft safety area. For the A320neo, a value of 7.5 m is used as the distance to the aircraft. This also applies for *HeRA*. Vehicles are only allowed to enter this area when the aircraft has come to a standstill and the wheel chocks are in position on the landing gears. 150 PAX enter *HeRA* through door 1L. A PBB can be used for door 1L. A rate of 20 PAX/min per door is assumed for deplaning. For boarding, the rate is 12 PAX/min per door. A time of 2 min is assumed for head-counting and last PAX seating allowance. For passenger handling, a time of 3.5 min is required for equipment positioning and removal, and opening and closing door [56]. Both galleys are located at door 1R which is served by a catering truck. A time of 2 min is required for opening doors and positioning equipment and a time of 1.5 min for closing the doors and equipment removal. A time of 1.2 min per trolley is required for trolley

exchange. An amount of 11 trolleys supplying the galley is assumed. Aircraft cleaning will be performed during free time while other operations take place.

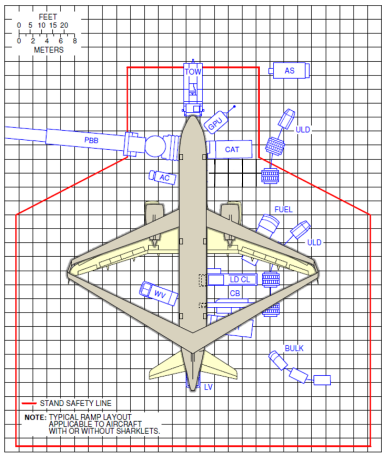

Figure 20: Ground handling compared to A320neo (yellow) with PBB [56]

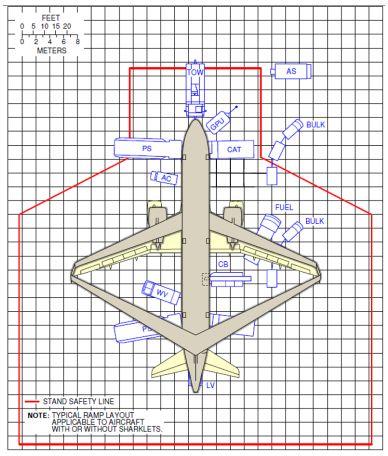

Figure 21: Ground handling compared to A320neo (yellow) [56]

HeRA does not carry any cargo containers, as such any vehicles serving the purpose of loading containers will not be needed. However, cargo space is still needed for the luggage of the passengers. A total of 3300 kg of baggage can be carried. For bulk loading a time of 120 kg/min for loading and 150 kg/min for unloading is estimated. The total loading time for bulk storage as such is 27.5 min and for unloading 22 min.
Assuming a volume flow of 900 l/min the largest tank of 23,000 l will take about 26 min to refuel. If parallel refueling of all tanks is used, refueling will take about 26 min. If all tanks are refueled after each other, refueling will take about 45.5 min which includes a time of 2.5 min for switching equipment between each tank.
A detailed breakdown of ground support times can be found in Table 19 in the appendix. Based on this a turnover time between 54 min and 1 h 13.5 min is expected. These values are calculated under the assumption that refueling will only start once all passengers have evacuated the aircraft and other ground operations like restocking of the galleys and loading and unloading of bulk storage will be carried out in parallel to refueling.

7 Conclusion

HeRA manages to comply with the key design parameters of being able to carry 150 passengers over a range of 2000 km. In addition, she demonstrates that a cryoplane utilizing LH_2 is feasible by 2035. *HeRA* makes use of innovative technologies which enable the possibility of more electric flight while also providing low emissions during its primary missions. Furthermore, she is able to fulfill these purposes while using conventional airport infrastructure, therefore requiring only minimal investment on part of the airports.
HeRA, with its evolutionary approach, provides familiar design features and visual components, such as a 2-engine turbofan configuration. This allows aircarriers to adopt the aircraft without worries, build confidence with the general populace through familiarity, while also integrating innovative design approaches to increase range and efficiency.

References

[1] McKinsey & Company. *Hydrogen-powered aviation A fact-based study of hydrogen technology, economics, and climate impact by 2050*. 2020.

[2] Cord-Christian Rossow, Klaus Wolf, and Peter Horst. *Handbuch der Luftfahrzeugtechnik*. HANSER, 2014.

[3] U.S Department of Energy. *Comparison of Fuel Cell Technologies*. 2011. URL: https://web.archive.org/web/20130301120203/http://www1.eere.energy.gov/hydrogenandfuelcells/fuelcells/pdfs/fc_comparison_chart.pdf (visited on 05/01/2021).

[4] Peter von Böck and Thomas Wetzel. *Wärmeübertragung Grundlagen und Praxis*. Springer, 2015.

[5] S.A Sherif et al. *Handbook of Hydrogen energy*. CRC Press, 2014.

[6] G. Dahl and F. Suttrop. "Engine control and low-NOx combustion for hydrogen fuelled aircraft gas turbines". In: *Int. J. Hydrogen Energy* 23 (1998).

[7] Felix Stoffels. *Die Tupolev, die bereits vor 32 Jahren mit Wasserstoff flog*. 2020. URL: https://www.aerotelegraph.com/tu-155-sowjetunion-die-wasserstoff-tupolev-die-bereits-in-1980er-jahren-flog (visited on 06/26/2021).

[8] European Union Aviation Safety Agency. *CS-25 Large Aeroplanes*. 2020. URL: https://www.easa.europa.eu/certification-specifications/cs-25-large-aeroplanes (visited on 07/03/2021).

[9] Arlind Pape. *Analyse der neuen LTH-Methode zur Massenschätzung von Flugzeugbaugruppen*. 2018. URL: https://www.repo.uni-hannover.de/handle/123456789/4319 (visited on 07/01/2021).

[10] Fahad Aman Khan. *Preliminary Aerodynamic Investigation of Box-Wing Configurations using Low Fidelity Codes*. 2010.

[11] R. Naveen. "Aerodynamic Analysis of C-Wing Aircraft". In: *INCAS* (2018).

[12] I. Kroo. *Nonplanar Wing Concepts for Increased Aircraft Efficiency*. 2005. URL: https://lf5422.com/wp-content/uploads/2014/08/vki_nonplanar_kroo-1.pdf (visited on 06/15/2021).

[13] Paul Olugbeji Jemitola. "Conceptual Design and Optimization Methodology for Box Wing Aircraft". PhD thesis. School of Aerospace Engineering, Cranfield University, 2012.

[14] D. Schiktanz and D. Scholz. *Box Wing Fundamentals - An Aircraft Design Perspective*. 2011. URL: http://www.fzt.haw-hamburg.de/pers/Scholz/Airport2030/Airport2030_PUB_DLRK_11-09-27.pdf (visited on 06/18/2021).

[15] D. Schiktanz. *Conceptual Design of a Medium Range Box Wing Aircraft*. 2011. URL: https://www.fzt.haw-hamburg.de/pers/Scholz/arbeiten/TextSchiktanzMaster.pdf (visited on 06/04/2021).

[16] *About OpenVSP*. URL: http://openvsp.org/learn.shtml (visited on 06/26/2021).

[17] D. Schiktanz and D. Scholz. *Das Boxwing-Flugzeug*. 2012. URL: http://www.fzt.haw-hamburg.de/pers/Scholz/Airport2030/Airport2030_ART_Ingenieurspiegel_12-05-15.pdf (visited on 06/18/2021).

[18] *Airfoiltools: NACA2412*. 2021. URL: http://airfoiltools.com/airfoil/details?airfoil=naca2412-il (visited on 06/21/2021).

[19] D. Schiktanz and D. Scholz. *Forces and moments acting on box wing*. 2011. URL: https://www.fzt.haw-hamburg.de/pers/Scholz/Airport2030/Airport2030_PUB_CEAS_11-10-24.pdf (visited on 06/01/2021).

[20] McKinsey. "Hydrogen-powered aviation, A fact-based study of hydrogen technology, economics, and climate by 2050". In: *script 20/21* ().

[21] Ian H. Bell et al. "Pure and Pseudo-pure Fluid Thermophysical Property Evaluation and the Open-Source Thermophysical Property Library CoolProp". In: *Industrial & Engineering Chemistry Research* 53.6 (2014), pp. 2498–2508.

[22] Jr. William E. Acree and James S. Chickos. *Thermophysical Properties of Fluid Systems in NIST Chemistry WebBook, NIST Standard Reference Database Number 69*. 2021. URL: https://doi.org/10.18434/T4D303 (visited on 07/01/2021).

[23] Thomas Wallner et al. "Fuel economy and emissions evaluation of BMW Hydrogen 7 Mono-Fuel demonstration vehicles". In: (2008).

[24] N.N. *Liquid Hydrogen Fuelled Aircraft - System Analysis*. 2003.

[25] Fatih Tunca and Nervzet Kaya. "Thermodynamic Analysis of Gas Turbine - Solid Oxide Fuel Cell(GT-SOFC) Aircraft Auxiliary Power Unit(APU)". In: *Journal of Advances in Mechanical & Automobile Engg.* (2017).

[26] Kristof Risse, Katharina Schäfer, and Florian Schültke. *CeRAS - Central Reference Aircraft data System*. 2021. URL: http://ceras.ilr.rwth-aachen.de/trac/wiki/CeRAS/AircraftDesigns/CSR01/Systems/EnergySinks (visited on 04/28/2021).

[27] Shuai Ma et al. "Fuel cell-battery hybrid systems for mobility and off-grid applications: A review". In: *Renewable and Sustainable Energy Reviews* (2021).

[28] Willy J.G. Bräunling. *Flugzeugtriebwerke*. Springer Vieweg, 2015.

[29] DLR. *NASA/DLR Aeronautical Design Challenge 2021*. 2020.

[30] *Wirkungsgrad*. URL: https://www.energie-lexikon.info/wirkungsgrad.html (visited on 07/13/2021).

[31] Reiner Korthauer. *Lithium-Ion Batteries: Basics and Applications*. 2017.

[32] Stefan Salchenegger. *Emissionen von Wasserstofffahrzeugen*. 2006. URL: https://www.umweltbundesamt.at/fileadmin/site/publikationen/REP0012.pdf (visited on 05/28/2021).

[33] TÜV SÜD. *Eigenschaften von Wasserstoff*. 2006. URL: https://www.tuvsud.com/de-de/indust-re/wasserstoff-brennstoffzellen-info/wasserstoff/eigenschaften-von-wasserstoff (visited on 05/29/2021).

[34] Anthony J. Colozza. *Hydrogen Storage for Aircraft Applications Overview*. 2002. URL: https://www.researchgate.net/publication/24316784_Hydrogen_Storage_for_Aircraft_Applications_Overview/link/0deec535eac638f679000000/download (visited on 06/22/2021).

[35] Felix Heubner and Lars Röntzsch. *Solid Hydrogen Carriers, Advanced metal hydride technology for hydrogen storage and compression applications*. 2021. URL: https://www.ifam.fraunhofer.de/de/Institutsprofil/Standorte/Dresden/Wasserstofftechnologie/Download_Whitepaper1.html (visited on 06/22/2021).

[36] Hannes Rienecker, Andreas Hauffe, and Klaus Wolf. *Abschlussbericht zum Vorhaben Optitube (Entwicklung von Optimierungsmethoden für Tragflügel mit zu Integralröhrentanks aufgelöster Holmstruktur)*. Tech. rep. Technische Universität Dresden, Institut für Luft- und Raumfahrttechnik, 2019.

[37] Martin Oehlke. *Masseabschätzung eines Wasserstoff-Außentanks für ein Turboprop-Verkehrsflugzeug*. 2009. URL: https://www.fzt.haw-hamburg.de/pers/Scholz/arbeiten/TextOehlkeMasse.pdf (visited on 07/01/2021).

[38] Gary L. Mills, Brian Buchholtz, and Al Olsen. *Design, fabrication and testing of a liquid hydrogen fuel tank for a long duration aircraft*. 2012. URL: https://aip.scitation.org/doi/pdf/10.1063/1.4706990 (visited on 07/02/2021).

[39] Thomas Longden et al. "Green hydrogen production costs in Australia: implications of renewable energy and electrolyser costs". In: *CCEP Working Paper* 20-07 (2020).

[40] Michael J Sefain. "Hydrogen Aircraft Concepts & Ground Support". PhD thesis. Cranfield University, 2006.

[41] C. Stiller et al. "Airport Liquid Hydrogen Infrastructure for Aircraft Auxiliary Power Units". In: *18th World Hydrogen Energy Conference (WHEC 2010)* (2010).

[42] U. Schmidtchen et al. "Hydrogen aircraft and airport safety". In: *Renewable and Sustainable Energy Reviews* 1.4 (1997), pp. 239–269.

[43] Caleb Amy and Alex Kunycky. *Hydrogen as a Renewable Energy Carrier for Commercial Aircraft*. 2019. arXiv: 1910.05632 [physics.gen-ph].

[44] K. Wolf. "Script Luftfahrzeugauslegung". Script of the Lecture "Conceptual Aircraft Design", Dresden University of Technology. 2019.

[45] Susanne Marquart et al. *Estimate of the climate impact of cryoplanes*. 2000.

[46] Nurettin Tekin et al. "Enhancement of fuel flexibility of industrial gas turbines by development of innovative hydrogen combustion systems". In: *gas for energy* 2/2018 (2018).

[47] *How are aircraft CO2 emissions calculated?* URL: https://www.verifavia.com/greenhouse-gas-verification/fq-how-are-aircraft-co2-emissions-calculated-11.php (visited on 07/13/2021).

[48] Paula Kurzawska and Remigiusz Jasi ´nski. "Overview of Sustainable Aviation Fuels with Emission Characteristic and Particles Emission of the Turbine Engine Fueled ATJ Blends with Different Percentages of ATJ Fuel". In: *Energies* 14 (2021).

[49] *NOx Emissions*. URL: https://www.umweltbundesamt.at/fileadmin/site/publikationen/REP0012.pdf (visited on 07/17/2021).

[50] J. Thorbeck. *DOC-Assessment Method, TU Berlin - DOC Method*. 2013. URL: https://www.fzt.haw-hamburg.de/pers/Scholz/Aero/TU-Berlin_DOC-Method_with_remarks_13-09-19.pdf (visited on 06/12/2021).

[51] Hydrogen Council. *Path to hydrogen competitiveness - A cost perspective*. 2020.

[52] *Airbus Aircraft 2018 Average List Prices*. 2018. URL: https://www.airbus.com/content/dam/corporate-topics/publications/backgrounders/Airbus-Commercial-Aircraft-list-prices-2018.pdf (visited on 06/12/2021).

[53] Airline Data Project. *Aircraft and Related*. URL: https://web.mit.edu/airlinedata/www/Aircraft&Related.html (visited on 06/12/2021).

[54] Xiaojia Zhao, J.C. Verhagen, and Richard Curran. "Disposal and Recycle Economic Assessment for Aircraft and Engine End of Life Solution Evaluation". In: *applied sciences* 10 (2020).

[55] *Reported Operating Cost and Utilization of Narrow-body Jets*. URL: https://www.planestats.com/bhsn_2018dec (visited on 06/13/2021).

[56] *Aircraft Characteristics, Airport and Maintenance Planning*. 2005. URL: https://www.airbus.com/aircraft/support-services/airport-operations-and-technical-data/aircraft-characteristics.html (visited on 06/26/2021).

A Appendix

A.1 Reference Plane

Table 16: Initial values of the reference plane

Properties	A320neo
Length	37.57 m
Wingspan	34.1 m
Wing area	122.6 m^2
Accommodations	150 PAX
Oswald efficiency number	0.76
Zero-lift drag coefficient	0.019
Specific fuel consumption	0.565 lb/lbf
Initial cruise altitude	36,000 ft
Normal operating speed	0.7 Ma

A.2 Aerodynamics

Table 17: Aerodynamic parameters of *HeRA* and A320neo

Parameter	*HeRA*	A320neo
Λ	9.69	9.48
b	34.1 m	34.1 m
S	120 m^2	122.6 m^2
ϕ	25°	25°
h/b	0.2	–

A.3 Mission Analysis

Table 18: Parameters used for the direct operating cost analysis

Parameter	Value
Plane price per kg of OEW	1150 €
Plane price per kg of engine mass	2500 €
Residual value factor	10%
Depreciation period	14 years
Insurance rate	0.5%
Interest rate	5%
Average yearly salary of flight attendants	60,000 €
Average yearly salary of cockpit crew (2 pilots)	300,000 €
Crew complement	5
Fuel price	3 €/kg [39]
Landing fees per MTOW	0.01 €/kg
Handling fees per MTOW	0.1 €/kg
ATC price factor	1.0
Cost burden	2
Labor rate	50 €/h
Yearly operation time	6012 h
Flight time	3 h
Block time supplement per flight	2.5 h

Table 19: Ground support times for *HeRA*

Passengers	
opening doors + equipment positioning	2 min
deplaning	7.5 min
boarding	12 min
closing door + equipment removal	1.5 min
Cargo	
Bulk loading	27.5 min
Bulk unloading	22 min
Refueling	
Equipment positioning	2.5 min
Fuel transfer	26 min - 38 min
Equipment changes between tanks	3 * 2.5 min
Equipment removal	2.5 min
Catering	
Equipment positioning + opening doors	2 min
Loading	13.2 min
Closing doors and equipment removal	1.5 min
Total	54 min - 1 h 13.5 min

A.4 Cabin Configuration

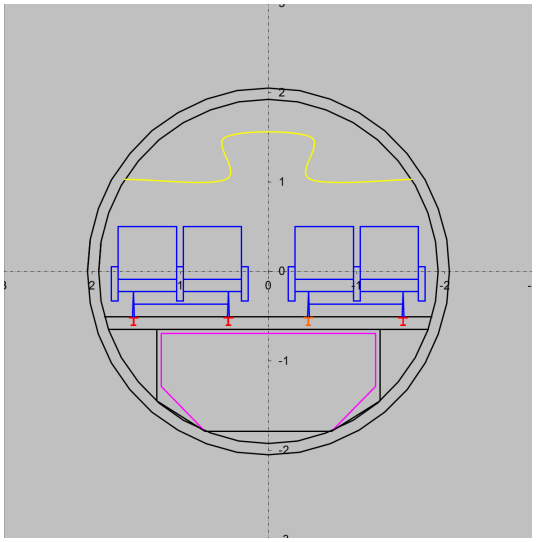

Figure 22: Cross section of cargo compartment with optional business class

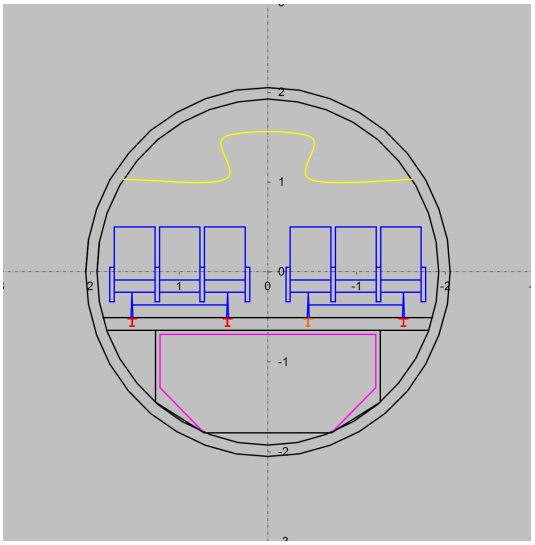

Figure 23: Cross section of cargo compartment with economy class

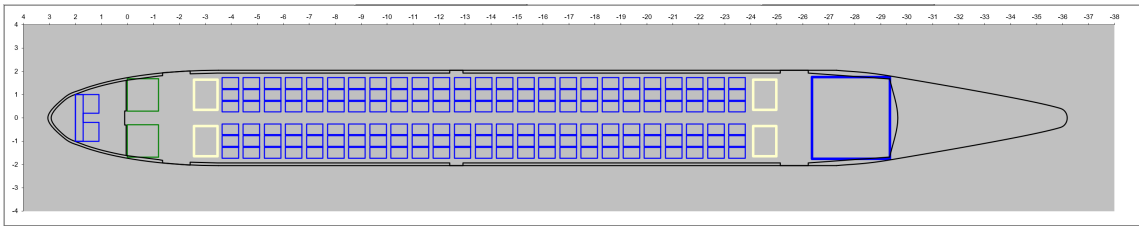

Figure 24: One-class cabin layout (150 PAX) - Green: galley; Yellow: lavatories; Blue behind cabin: aftward H_2 tank

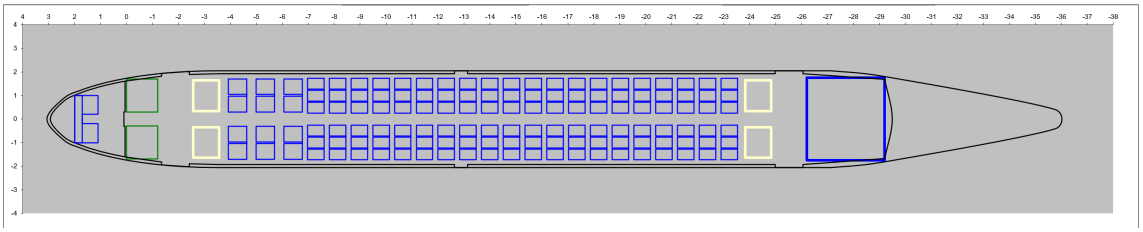

Figure 25: Optional two-class cabin layout (12 FC/ 120 EC seats)

A.5 V-n Diagram

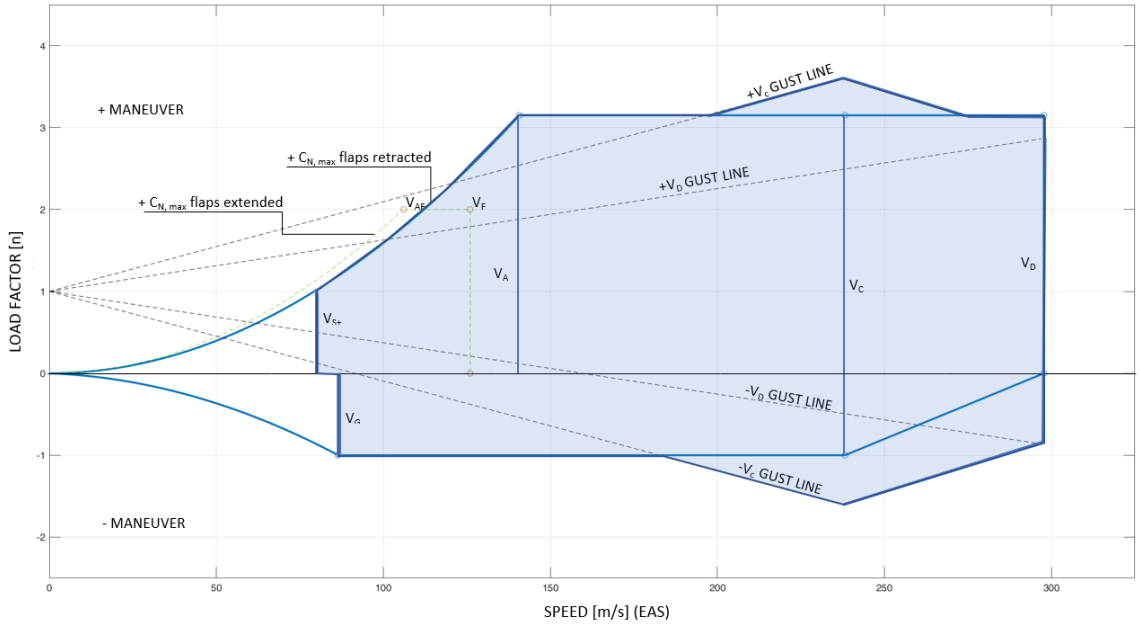

Figure 26: V-n diagram with maneuver boundaries

A.6 Plane Parameters

Table 20: *HeRA* parameters

Parameter	Value
Mass	
Fuselage	9200 kg
Wing/box wing	9000 kg
VTP	870 kg
Nacelles & pylon	1500 kg
Landing gear	3000 kg
Cryotank	3800 kg
Tank insulation	600 kg
Tank system	2000 kg
Structural Weight	**29970** kg
Operational items	5300 kg
Propulsion group	7200 kg
Furnishings	2900 kg
Aircraft systems	4700 kg
Operational Empty Weight	**50070** kg
Max. payload	15750 kg
Max. fuel	2300 kg
Maximum Take-Off Weight	**68120** kg
Payload for design mission (2000 km)	15750 kg
Fuel, including reserve, for design mission (2000 km)	2300 kg
Take-Off Weight Design Mission (2000 km, 150 PAX)	**67540** kg
Fuel, including reserve, for design mission (600 km)	830 kg
Take-Off Weight Design Mission (600 km, 150 PAX)	**66650** kg
Size	
Cabin	
Width	3.76 m
Length	25.04 m
Fuselage	
Width	3.96 m
Height	10 m
Length	38.98 m
Wing	
Wingspan	34.1 m
Depth root	2.81 m
Depth tip	0.7 m
Area	120 m^2
Aspect ratio	9.69
Dihedral (top)	0°
Dihedral (bottom)	9°
Sweep (top)	-25°
Sweep (bottom)	25°
Taper	0.25
Tail	
Root length	5.11 m
Tip length	2.26 m

Table 20: *HeRA* parameters

Parameter	Value
Height	3.07 m
Width	0.36 m
Area	22.6 m^2
Aerodynamics	
e_{cruise} (Oswald factor)	1.1637
E_{Cruise}	19.69
$C_{L,cruise}$	0.86
$C_{D,0}$	0.019
E_{opt}	21.59
$\frac{h}{b}$	0.2
$\frac{t}{c}$	0.119
α_0	-2.5°
Engines	
Amount	2
F_0	130 kN
Cabin Layout	
Seating configuration	3-3
Economy seats	150
Economy rows	25
Aisle width	0.5 m
Seat pitch	0.81 m
Economy toilets	4
Economy galleys	2

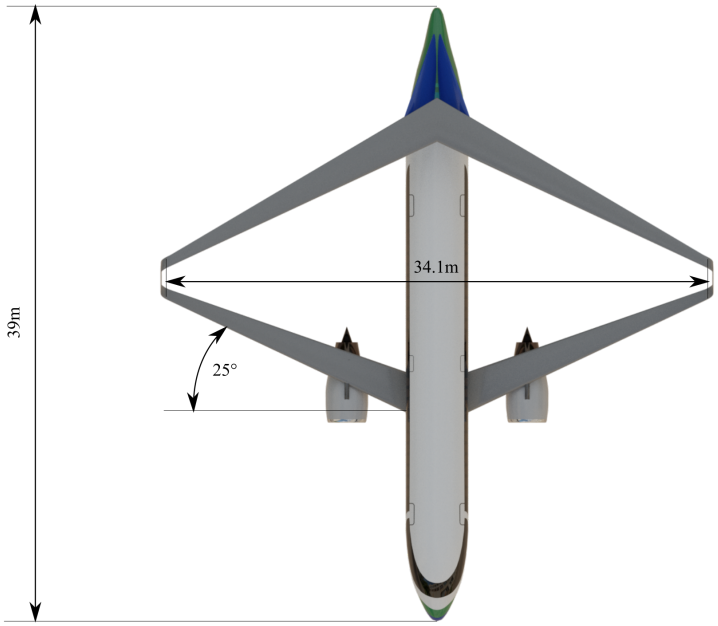

Figure 27: Measures of *HeRA* (top-down)

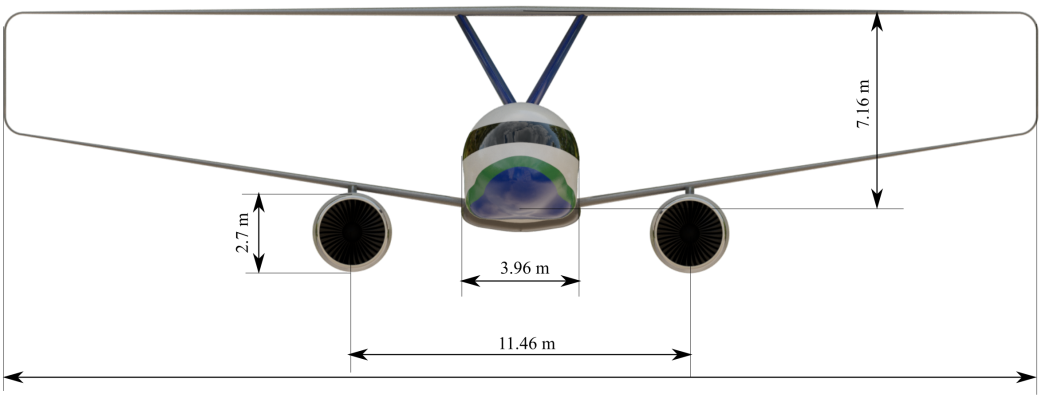

Figure 28: Measures of *HeRA* (front)

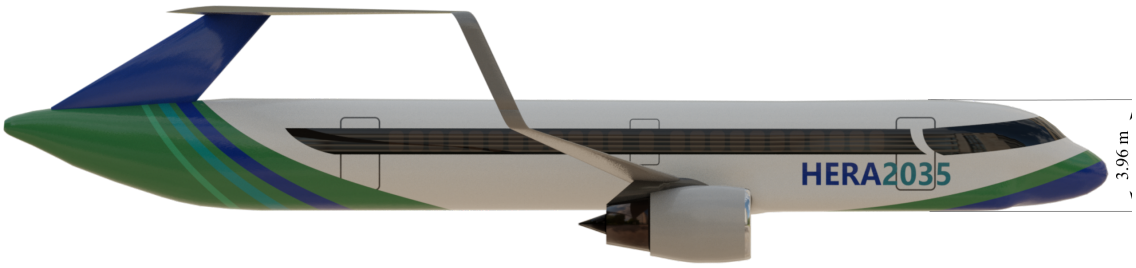

Figure 29: Measures of *HeRA* (side)

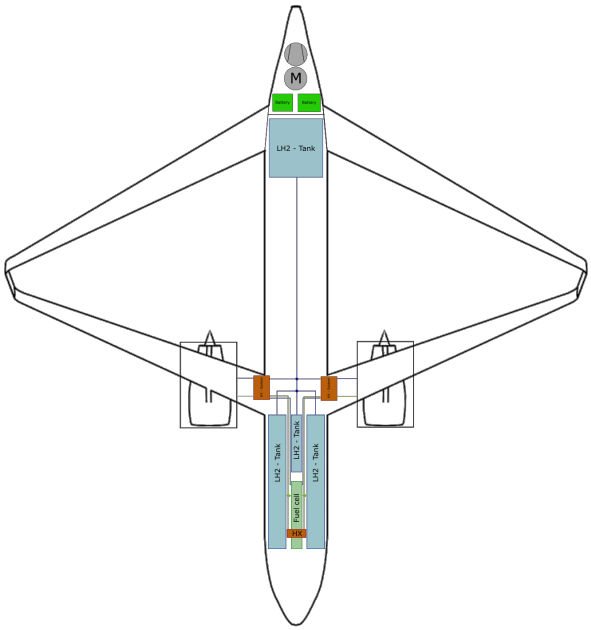

Figure 30: System layout of *HeRA*

A.7 Stringers and Frames

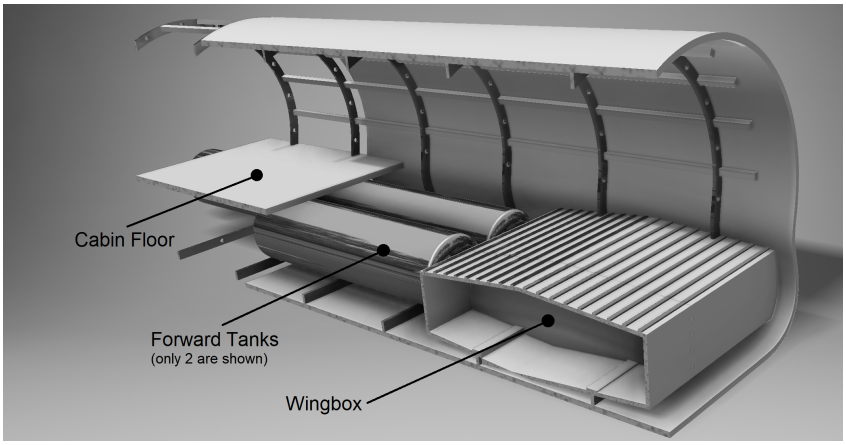

Figure 31: Schematic visualisation of front fuselage section

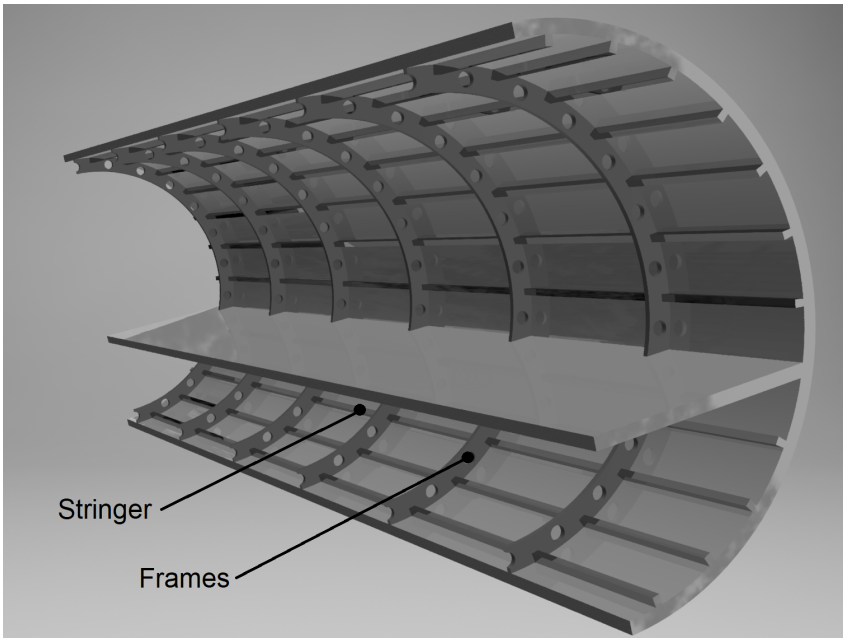

Figure 32: Schematic visualisation of aft fuselage section

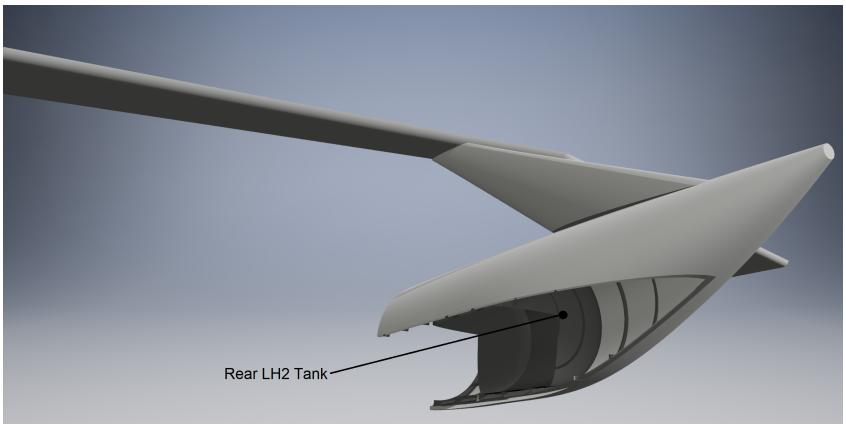

Figure 33: Schematic visualisation of tail fuselage section

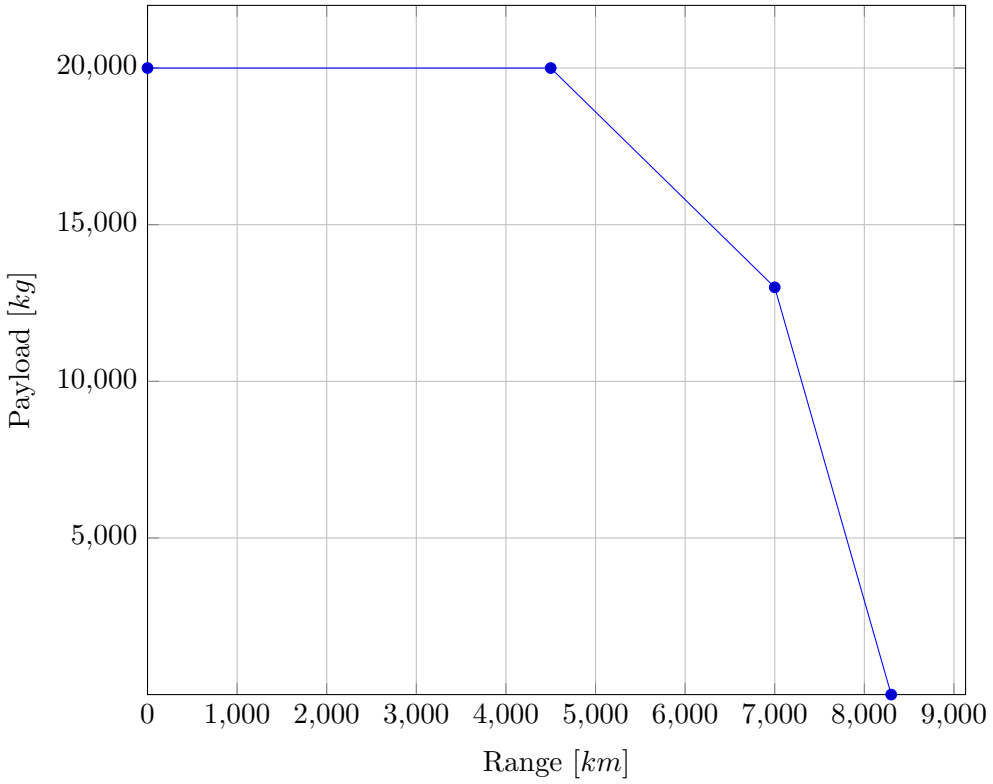

Figure 34: Payload range diagram of A320neo

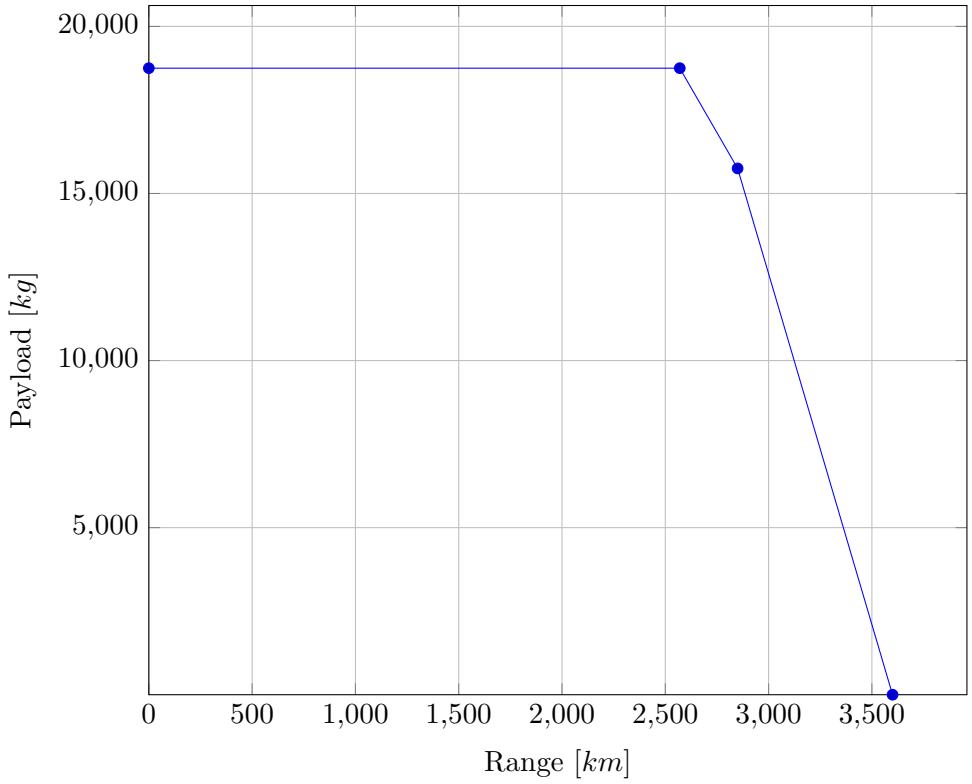

Figure 35: Payload range diagram of *HeRA*

A.8 Mission Analysis Approach

The segments of the flight are defined as follows:

- ascend from 1,500 ft to 10,000 ft with a constant CAS of 250 kt
- at 10,000 ft acceleration to V_{Climb} (TAS)
- ascend from 10,000 ft with a constant CAS of V_{Climb}(TAS) until the crossover altitude is reached where the Mach number equals the cruise Mach number Ma_{Cr}
- ascend from crossover altitude with Ma_{Cr} until the initial cruise altitude (ICA) is reached
- cruise with Ma_{Cr}, with a small increase in height due to decreasing aircraft weight
- descend with Ma_{Cr} until the crossover altitude is reached where the CAS equals the desired CAS for descent (e.g. 270 kt)
- descend from crossover altitude with constant CAS until a height of 10,000 ft is reached
- at 10,000 ft deceleration to 250 kt (CAS)
- decrease from 10,000 ft with a constant CAS until a height of 1,500 ft is reached

Below, the method used is exemplary explained for the cruise segment. For the ascend and descend segments, the calculations are more complicated since the instationary vertical motion has to be taken into account, while there are simple horizontal and vertical force equilibria in the cruise segment. At the beginning, a step with Δs is defined. Afterward, a loop is executed. At the beginning of each iteration, the air density $\rho(h)$ and the sonic speed $a(h)$ are computed using the standard atmosphere. Then, the aircraft´s TAS

$$V_{TAS} = Ma_{cruise} a(h) \tag{11}$$

is calculated. Afterward, the increased height due to the decreasing aircraft mass h is determined by evaluating the vertical force equilibrium:

$$C_L \rho(h) V_{TAS}^2 S = 2mg \tag{12}$$

m being the current aircraft mass. In the cruise segment, the thrust equals the drag so the aircraft is neither accelerated nor decelerated. Therefore,

$$F = \frac{1}{2} C_D \rho(h) V_{TAS} S \tag{13}$$

Now, the time needed for the step can be expressed as

$$\Delta t = \frac{\Delta s}{V_{TAS}} \tag{14}$$

and the mass reduction can be expressed as

$$\Delta m = -b_F F \Delta t \tag{15}$$

b_f being the specific fuel consumption. With the new mass, the next iteration is computed.

A.9 Powertrain

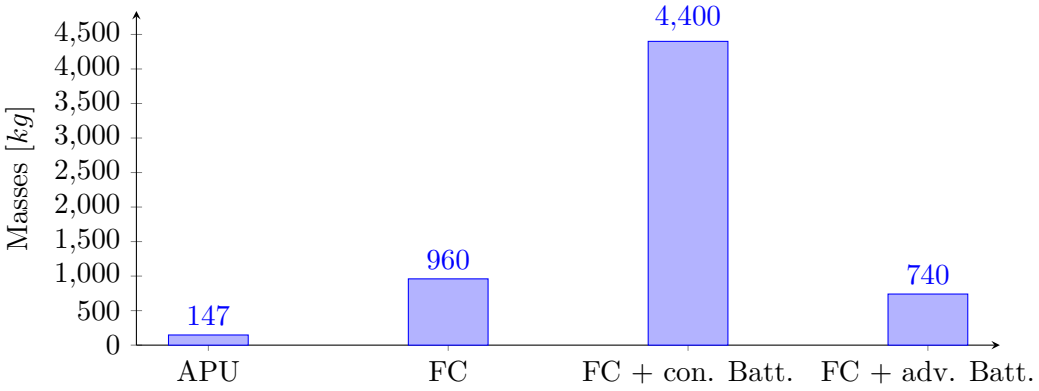

Figure 36: Configuration masses

A.10 Design Algorithm

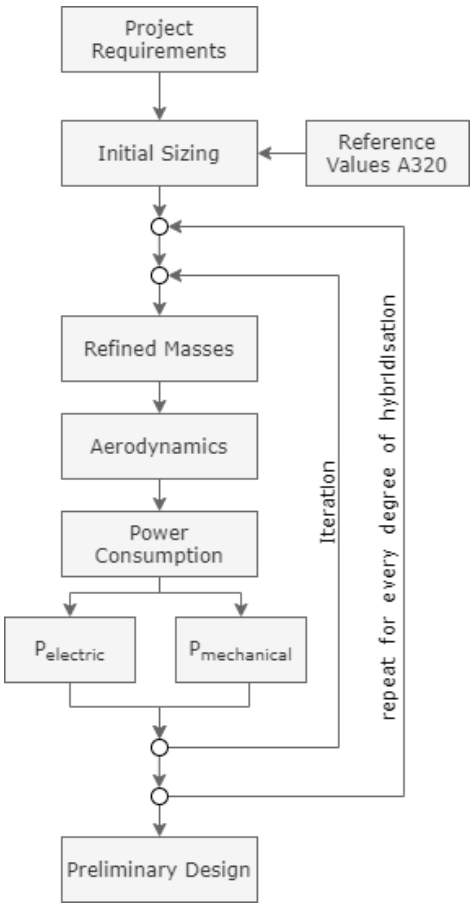

Figure 37: Preliminary design algorithm